

# Reply *(in blue)* to Referee #1

---

**We thank the referee #1 for the positive assessment of the paper.**

*Our reply is included after the referee comments.*

1. The paper describes a novel method to derive the geometry dependent Lambert Equivalent Reflectance of the Earth scene, which is an important parameter needed for the retrieval of trace gases. The method is shown to have many benefits over the use of a climatology, as has been used often for past missions. The introduction of the paper is well written and of good quality, nonetheless, the remainder of the paper is a bit thin when it comes to provide evidence of the improvements over existing climatologies. Only comparisons with OMI are given while there exists more climatologies based on other missions. Also the directional aspect of the GE\_LER needs more validation. The paper covers new and interesting topics and techniques, and after the comments (some of which major) and corrections have been adequately addressed, the paper could certainly be published.

*In the updated paper (new Section 4.4) we include comparisons with OMI and GOME-2 LER*

2. Although the paper stresses the importance of the inclusion of BRDF in the newly derived TROPOMI surface reflectivity, this is not the only factor that plays a role, and probably not the strongest factor. Since the radiation field in the UV is largely diffuse, the actual BRDF of the surface is not so important. The better inclusion of snow/ice areas and the higher spatial resolution probably play a stronger role. Please discuss this point, and try to separate the effects of the three factors: BRDF, snow/ice, and spatial resolution in the comparison of TROPOMI GE-LER with OMI-LER climatology. The improvement that is found in the TROPOMI total ozone retrieval in Fig. 11 when using the TROPOMI GE-LER instead of the OMI-LER is apparently due to the better snow/ice mapping at high latitudes, not to BRDF effects.

*The reviewer is certainly right; in the UV the main improvements are from the accurate snow/ice retrievals whereas in the VIS the BRDF effects are stronger.*

*To better balance the different benefits from GE\_LER we have:*

- *Remove BRDF from the title, the new title is “Applying FP\_ILM to the retrieval of geometry-dependent effective Lambertian equivalent reflectivity (GE\_LER) daily maps from UVN satellite measurements”*
- *Emphasize in the introduction and conclusions the advantages of retrieving daily surface properties (especially important for snow/ice conditions) with the same spatial resolution and the same fitting window as the trace gases.*

3. Are the GE\_LER data available to the community? Please specify whether and how you plan to distribute the GE\_LER and G3\_LER data products. In order for other people to reproduce your results and claims they need open access to the data presented in this paper.

The retrieved GE\_LER and the G3\_LER used for each single TROPOMI ground pixel will be included in the operational S5P total ozone product. All operational S5P products are open and free available. We will discuss with ESA/EU the possibility of disseminating the G3\_LER total ozone daily maps in the same way as the operational S5P products.

**4.** Which are the wavelengths for which GE\_LER is retrieved? In the paper it is not so clear for which wavelength the results apply. For instance, only in the caption of Figure 6 this is mentioned.

As mentioned in the Introduction and Conclusions, the GE\_LER/G3\_LER algorithms can be applied to any wavelength region. The examples shown for S5P are for the total ozone fitting window and the corresponding wavelengths are given in the first sentence of section 4 “...using the fitting window of 325-335 nm”.

Additionally we added the fitting window information for the S5P examples in Section 4.2 and in the Conclusions.

### Specific comments

**1 p1** The title is hardly readable due to the many acronyms. Please make the title clearer. In the rest of the paper the construction “FP\_ILM GE\_LER” is hardly readable. Can you think of a better name?

We simplified the title by removing the BRDF part. See the reply to the general comment#2

FP\_ILM GE\_LER together is indeed hard to read; in the updated paper we use only GE\_LER.

**2 p2 116** These are not fundamental problems of a climatology itself, but rather information missing in the currently available climatologies. It would definitely be possible to create a climatology that includes the viewing angle dependency, or address separately snow and snow-free conditions.

That is correct, the sentence is reformulated to “common problems with typical LER climatologies”

**3 p3 115** The drawbacks mentioned for lookup tables are not very convincing, consider rephrasing this sentence.

This sentence reads now “The main drawbacks of look-up tables representing high dimensional RTM simulations (common in atmospheric composition retrievals) are that the memory requirements increase exponentially with the number of input dimensions, the interpolation/extrapolation in this multi-dimensional space are computationally expensive, and the interpolation/extrapolation errors could be significant.”

**4 p4 18** The smart sampling technique should be explained in a bit more detail because readers may not want to read the full paper referred to.

The following text is included in Section 2.2. “Training data is traditionally created at fixed intervals uniformly distributed for each input variable; as a consequence the training samples are grouped around the node points and a very poor coverage of the multidimensional input space is reached. Deterministic sampling methods provide a more uniform distribution of the training data covering the entire space of each input variable” and “For this work we select a Halton sequence that uses prime numbers for creating sample points in each input dimension and a radiative transfer model computes the corresponding simulated radiances”.

**5 p4 116** I do not understand this sentence: “Machine learning techniques perform best with low-dimensional datasets by avoiding the effects of the curse of dimensionality.”

This second part of the sentence “by avoiding the effects of the curse of dimensionality” is removed.

**6 p5 127** What about the azimuth dependence of  $\rho$ ? This also holds for other places in the paper. Please clarify in Sect. 2 how you deal with the solar zenith angle and relative azimuth dependence of the BRDF.

The following clarification is included in Section 3 “solar zenith angle dependencies can be ignored when combining GE\_LER data from Sun-synchronous satellites over the same position because the angle of sunlight upon the Earth's surface is consistently maintained. Likewise relative azimuth angle dependencies are negligible in the UV.”.

**7 p7 19** How did you calculate the standard deviation, is it based on all simulations in the validation training set? Figure 5 on page 22 seems to indicate larger errors (up to 0.01) for individual LER retrievals. What are these red error bars in this figure? How does this error propagate in the final accuracy of the trace gases?

Correct, we use all simulations in the validation dataset.

The following clarification is included in section 4.1 “the x-axes are divided in bins and the mean and standard deviation (red bars) are calculated for each bin.”

The larger errors correspond to high SZA. The effects of LER errors on the trace gases accuracy is discussed in the first sentence of the Introduction.

**8 p7 115** Why do you use Z as symbol for pressure and not P? Z can easily be confused with height.

Thanks for pointing out this inconsistency. The retrieval is actually based on surface height and not pressure. The symbol  $Z$  is correct, the text in Section 2 and 4 is updated.

**9 p7 121** The histograms presented in Figure 7 are not discussed in detail.

In chapter 4 we include a new section describing the comparison with GOME-2 and OMI LER.

**10 p7 section 4.3 / Figure 9:** This should become a separate main section, with a thorough and complete validation of the product. The comparison that is presented is not sufficient. Comparisons can be performed with a number of the surface LER -databases that were mentioned in the introduction (OMI, SCIAMACHY, GOME-2), but also with BRDF information from MODIS. Using MODIS BRDF would mean adjusting the retrieval to retrieve wavelengths of the nearest MODIS band. Can this be done?

The main focus of this paper is to present the algorithms for obtaining G3\_LER and G3\_LER, the results for S5P total ozone are shown as demonstration.

In chapter 4 we include a new section describing the comparison with GOME-2 and OMI LER.

The MODIS BRDF is available only in the VIS. As explained in the Conclusions, GE\_LER retrievals in the VIS are planned for future work.

The differences have to be analysed properly. The difference plot in Figure 9(b) does not allow the reader to study differences on the order of 0.02, which is the typical difference/error one would expect for snow-free areas.

In chapter 4 we include a new section describing the comparison with GOME-2 and OMI LER.

**11 p8 12** “from the couple of days”: how many days did you use?

This sentence is reformulated as follows “The TROPOMI G3\_LER map for a given day is created by regriding (using a  $0.1^\circ \times 0.1^\circ$  resolution) the clear-sky LER data from the same day with the G3\_LER map based on the LER data from previous days”

**11 p8 111** Figure 8 needs more explanation, what order polynomial is used, what do the blue error bars represent? Why do land, water and snow scenes all have more or less the same relative albedo (around 1.0 – 1.6)? Have you calculated this average using all global pixels?

This implies that you have mixed different land types in the calculation of the average. How representative is the viewing angle dependency then for individual land types?

The data for each surface type are normalised relative to the central detector pixel (nadir) therefore the range is around 1. This explanation is included in Section 4.3 and Figure 8.

**12 p8 115** Please check which version of the OMI LER was used; the second version covers 5 years of data between 2005 – 2009, released in 2010.

The data used here are the 4 years data released in 2008. In an early stage of the S5P project we compared both the 2008 and the 2010 versions and found some systematic structures in the 2010 version especially in the 328 nm dataset. Therefore we decided to use 2008 version.

**13 p8** Which field of the OMI-LER is used to compare with? Is it the "MonthlyMinimumSurfaceReflectance" field or is it the "MonthlySurfaceReflectance" field?

We use the MonthlyMinimumSurfaceReflectance field.

**14 p11ff References:** please put all references in alphabetical order.

Done

**15 Fig 5** Did you also consider the sensitivity of the GE\_LER error due to ozone profile assumptions?

We are using ozone profile climatologies organized as function of the total ozone (the total ozone and the ozone profile are strongly correlated). Therefore the sensitivity of the GE\_LER to the ozone profiles is covered by the total ozone dependency.

**16 Fig 8** What do you mean with "relative mean albedo"? Can you please also provide the GE\_LER itself?

Please clarify, "relative mean albedo" is not mentioned in Fig. 8.

**17 Fig 19** These maps are not very informative because the dynamic range is too large. Please choose a color scale and albedo range that provides spatial information on the distribution of surface albedo in the UV.

Maps updated



# Reply (in blue) to Referee #2

---

**We thank the referee #2 for the constructive comments.**

Our reply is included after the referee comments.

This manuscript presents a new approach to derive effective scene albedo on a pixel per-pixel basis from TROPOMI observations and to build a viewing zenith angle dependent LER climatology with an improved spatial resolution compared to former data bases. Although the topic of the study fits well within AMT and there is no obvious issue with the approach, I would suggest to further discuss the results and to extend the comparisons to better demonstrate the added-value of the database. For example, results are discussed for only one spectral region and a limited amount of data (April 2018).

It would be beneficial to have more illustrations for different months. Reading the manuscript, I had many comments similar to those from reviewer 1. I won't list those again but encourage the authors to carefully reply to them. Below are a few additional comments. Once the comments have been addressed and the manuscript consolidated, this work will be worth being published within AMT.

As general reply we would like to highlight that the G3\_LER is not a climatology or database as commonly created by other methods but a dynamic map updated every day and in this way it represents the current surface conditions.

Furthermore, the main focus of this paper is to present the algorithms for obtaining G3\_LER and G3\_LER, the results for S5P UV (ozone) are shown as demonstration. Results for different seasons were already included in the submitted version, see for example Fig. 8.

## **Comments:**

- The description of the smart sampling and machine learning approaches is quite technical. It would be beneficial to the readers to further describe the general ideas/concepts on which rely those methods.

The following text is included in Section 2.2. *“Training data is traditionally created at fixed intervals uniformly distributed for each input variable; as a consequence the training samples are grouped around the node points and a very poor coverage of the multidimensional input space is reached. Deterministic sampling methods provide a more uniform distribution of the training data covering the entire space of each input variable”* and *“For this work we select a Halton sequence that uses prime numbers for creating sample points in each input dimension and a radiative transfer model computes the corresponding simulated radiances”*.

- Section 3: Could you provide more details here on how clear-sky pixels are selected? Such details are given later in the manuscript but it would good to already describe this in section 3. Could you also provide some statistics on the number of days required to have a global

coverage? There must be some regions with persistent clouds for which the update frequency drastically decreases. Actually, it would be useful for traceability to provide this information in the database along with the G3\_LER values. For example, for one given cell, the LER value has been derived from day-1, -2, -3, or . . .

TROPOMI and VIIRS data are used for the clear-sky determination. The following sentence is included in the paper: *“In the case of S5P, clear-sky is determined using both the operational cloud properties retrieved from TROPOMI (Loyola et al., 2018) and the VIIRS/SNPP (Visible Infrared Imaging Radiometer Suite sensor onboard Suomi National Polar-orbiting Partnership satellite) cloud mask regridded to the TROPOMI resolution (R. Siddans, 2016). Note that S5P and SNPP fly in loose formation, the S5P orbit trails 3.5 to 5 minutes behind SNPP”*

One month of data is usually enough for obtaining a globe map. The following explanation is added in section 3: *“The spatial resolution of the G3\_LER maps for TROPOMI is 0.1° and global maps can be generally derived combining data from one month. Two to three months of data are only needed for regions covered with persistent clouds like the Intertropical Convergence Zone (ITCZ).”*

The G3\_LER is not a classical static database, as explained in section 4.3 the G3\_LER maps are updated on a daily basis to represent the current surface conditions. To address the traceability question of the reviewer, we added the following in section 4.3: *“Time information (orbit number) of the LER used in each grid cell is included in the GE\_LER maps.”*

- G3\_LER data seems to be available only for the ozone fitting window and for three surface types. Could you comment why only those three surface have been considered? In other regions than UV, BRDFs effects will differ much more significantly as a function of the surface type. Could you clarify if you intend to provide GLER data in other spectral ranges and how you intend to proceed with respect to this aspect.

The selected land, water and snow/ice cover well the BRDF effects in the UV. We include the following sentence in section 4.3 *“Note that the selected surface types cover the BRDF effects in the UV ozone fitting window; other trace gases like NO<sub>2</sub> in the VIS will require different land cover types (e.g. water, snow/ice, urban, paddy, crop, deciduous forest, evergreen forest) to properly model the BRDF effects, see Noguchi et al., 2014.”*

Regarding the second question about the spectral ranges, in the Conclusions we already indicate our plans to apply the GE\_LER/G3\_LER to other S5P fitting windows.

- It is mentioned that the Bodeker ozone database is combined with the McPeters/Labow climatology as input of the RT simulations. Could you be more specific on the needs for this combination and on what is provided by each of those databases. Also in Table 1, the ozone profiles appear to be classified only as a function of the total column. Is it sufficient or are the geographic variations of the profiles accounted for somehow? Is there any latitude/longitude

dependence taken into account? If not, please be more specific on the profiles that have been used. Also could you provide typical sampling steps of the different dimensions?

The corresponding paragraph in section 4.1 was rephrased as follows: *“We use the Bodeker et al., (2013) database for representing the stratospheric ozone combined with the McPeters/Labow (Labow et al., 2015) climatology for the lower tropospheric ozone.”*

A classification as function of the total column is sufficient thanks to the strong correlation between the total ozone and the ozone profile shape.

The smart sampling does not use “sampling steps”. Please see our reply to your first comment.

- Figure 7: to better illustrate the possible impact of BRDF, could you show such clear-sky histograms for different range of viewing angles. If BRDF effect is important, we could expect systematic biases varying as a function of the VZA. Also, biases are more important for cloud cases. Is it because cloud albedo are retrieved in a different spectral region?

We created histograms as function of VZA but they are not really informative. The BRDF dependency on the VZA can be better appreciated in the plots from Figure 8.

- Figure 8 : what are the implications of the numerical instability of the RT simulations around VZA=0 on the retrieved LER?

We removed the numerical instability and created extra simulations around nadir (VZA=0).

- Figure 9: There is a clear general bias between the G3\_LER and OMI\_LER data, even at low/mid-latitudes. Could you better quantify and discuss this? Is there any indication that one of the two data sets would be more realistic?

We found out that the small bias was due to imperfections on the current TROPOMI L1 products. The following sentence was added in section 4.2 *“The version 1 of the TROPOMI Level 1 product has small deficiencies on the UV band; therefore a soft-correction based on comparisons with OMPS radiances is applied to S5P. It is expected that the version 2 of the TROPOMI Level 1 product will include a more accurate radiometric calibration”*.

We include a new section 4.4 describing the comparison with GOME-2 and OMI LER. However, it is not obvious which of the three data basis is actually best / most realistic. For some cases two of them agree well for other cases other two agree better.

**Minor/Technical comments:**

- Quality of figures is generally low. Could you increase the quality as well as the size of labels?

Figure quality and font size improved

.

- Page 2 – line 6: 35% on ozone column seems large. Is this value correct?

Figure 4 of Lerot et al. shows AMF changes in this magnitude when a surface albedo of snow/ice is used instead of surface albedo of water.

- Page 2 – line 12: Could you be more specific with that statement? Are there some references providing estimates of errors on TROPOMI products caused by the too coarse resolution of old databases?

Error estimates are not yet available, but this is a known data quality issue listed in the “Product Readme File” of the S5P L2 products, see <http://www.tropomi.eu/documents/prf>

- Page 3 – line 29: Add “solar and” before “viewing geometry”?

Done

- Page 6 – line 8: The LER data could still differ from the actual surface properties in case of sudden snow fall combined with significant cloudiness.

That is correct, at the end of the sentence we added “*The only exceptions are cases of sudden snow fall combined with significant cloudiness*”.

- Page 6 – line 16: remove “viewing geometry”

Done

- Figure 4 shows negative optical densities, which is not physical. In the text, those quantities are referred to optical densities differences but it is not clear what is the reference. Could you homogenize the text and y-label and clarify what are those optical density differences?

Negative optical densities are indeed misleading. What is shown here is the optical density of the DOAS polynomial ( $p(\lambda)$  in Equation 2). This information is added in Section 4.1 and in Figure 4.

- Page 7 – lines 5-6: This is very technical and the meaning is not clear at all for me. Could you rephrase this?

We use common nomenclature of machine learning; the text has been updated as follows:  
*“The best results are obtained using a feedforward NN (the neurons are grouped in layers) with a topology ...”*

- Page 8 – line 2: “from the couple of days” is not clear. Please be more specific.

This sentence is reformulated as follows *“The TROPOMI G3\_LER map for a given day is created by regridding (using a  $0.1^\circ \times 0.1^\circ$  resolution) the clear-sky LER data from the same day with the G3\_LER map based on the LER data from previous days”*

- Page 8 – line 29: “smoother” instead of “smother”

Done

- Page 9 – line 31: Mention that those numbers are valid for April 2018.

Done

# Reply (in blue) to Referee #3

---

We thank the referee #3 for the positive comments and for the detailed review of the paper.

Our reply is included after the referee comments.

Mateer et al. (1971) first proposed a Lambertian Equivalent Reflectivity (LER) concept in UV total ozone retrievals to account for combined spectral dependence of surface, aerosols and cloud reflectance [Mateer, et al., 1971]. The concept works well because ~90% ozone is in the stratosphere, above effective reflecting surface. The simple LER concept with some modifications (e.g. extrapolated LER spectral dependence, effective surface pressure) has been successfully used in heritage (TOMS, GOME, SCIAMACHY) and current (GOME-2, OMI, OMPS, S5P/TROPOMI) stratospheric ozone and other trace gases (e.g., volcanic SO<sub>2</sub>) UV retrievals. The need for satellite retrievals of tropospheric ozone and other pollution gases (NO<sub>2</sub>, SO<sub>2</sub>, HCHO) in partly cloudy scenes, with peak concentrations in or just above the planetary boundary layer, required modification of the simple LER concept, replacing it with the mixed-LER (MLER) concept: mixing two LER surfaces, one at the ground and the other at the effective cloud pressure, e.g., [Ahmad, et al., 2004; Stammes, et al., 2008]. The MLER approach is currently used in operational UV pollution gas retrievals (e.g., [Levelt et al., 2018] and references therein). The MLER approach requires a-priori “clear-sky” LER estimate, which can be taken either from concurrent satellite measurements (e.g., OMI geometry-dependent GLER product uses higher-resolution atmospherically corrected MODIS BRDF [Vasilkov et al., AMT 2017]) or from prior measurements (e.g., OMI cloud-cleared climatological LER [Kleipool et al., JGR 2008]). The climatological “clear-sky” LER estimation is less accurate, since it disregards the observational geometry- and time-dependence of surface reflectance. The paper by Loyola et al. presents new geometry-dependent (GE-LER) LER implementation, the "Full Physics – inverse Learning Machine (FP\_ILM)" algorithm and the multiple day gridded LER product (G3\_LER) derived from the present and previous clear-sky scenes observed by S5P/TROPOMI. In previous LER implementations for ozone retrievals, the LER values were derived at non-absorbing wavelengths (e.g., 340nm and 380nm for Nimbus-7 TOMS) and spectrally interpolated to the ozone and SO<sub>2</sub> retrieval windows. The important advantage of the new GE-LER retrieval is that it is retrieved in the same spectral fitting window used by ozone retrieval (325-335nm), thus does not require spectral extrapolation. This is the first simultaneous retrieval of both ozone and LER in this spectral window. The G3\_LER can be applied to existing S5P aerosol, clouds and trace gas algorithms by replacing climatological clear-sky LER with the new G3\_LER product. I recommend publishing the paper with clarifications and technical corrections and releasing the new S5P GE\_LER and gridded G3\_LER products for community evaluation.

We include now references to Mateer et al. and Ahmad et al. in the Introduction.

## General comments

1) The name “full physics” is misleading, because the forward radiative transfer model used for NN training does not include important physical processes, such as , aerosols and inelastic (RRS) scattering;

The goal is to retrieve the surface properties under clear-sky conditions, therefore the RTM simulations don't consider modelling of aerosols or clouds.

The impact of using RSS in the forward simulation for the GE\_LER retrieval in the ozone fitting window is negligible. We add the following in Section 4.1 *“The mean difference in GE\_LER retrievals based on LIDORT-RSS and VLIDORT is in the range of  $5e-5$  for  $SZA < 75^\circ$  and  $3.5e-4$  for larger SZA”*.

2) acknowledge that BRDF effects on trace gas retrievals cannot be modeled exactly using forward RTM with Lambertian surface. Estimate the ozone errors due to Lambertian surface assumption (GE\_LER or simple LER) using BRDF supplement available in VLIDORT RTM.

The following sentence is included at the end of Section 4.1 *“The BRDF effects on the ozone fitting window are well modelled using the GE\_LER approximation, the difference in the total ozone retrieved using VLIDORT and VLIDORT-BRDF simulations is in the order of 0.5 DU or 0.2%”*.

3) Provide more details about GE\_LER algorithm:

a. Do you assume that GE\_LER is wavelength independent within DOAS fitting window?

Correct, we listed this assumption in Section 2.3.

b. Give reference to the machine learning (NN) software and explain selecting optimal NN topology used in the algorithm training.

We use the MATLAB neural network Toolbox. The following explanation is included in Section 4.1 *“Different NN topologies were tested using one, two, and three hidden layers”*.

c. Clarify whether the RTM with Lambertian surface or with BRDF model was used for training?

As already indicated in Section 4.1, we use the VLIDORT model with Lambertian surface.

d. Explain which cloud masking algorithm was used in creating G3\_LER clear-sky daily map

We add the following explanation in Section 4.3 *“we use the S5P OCRA and the VIIRS/SNPP (flying in constellation with S5P) cloud fractions  $f_c$  for identifying clear-sky measurements.”*

e. Fig. 1– clarify that “simulated features” are DOAS ozone slant columns and polynomial closure coefficients.

Fig. 1 is the general scheme for the FP\_ILM training phase. The particularities for each GE\_LER step (e.g. VLIDORT used as forward model, NN used as machine learning, DOAS used as feature extraction) are described in Sections 2.1 to 2.4.

f. Fig. 2 – clarify that “extracted features” are DOAS ozone slant columns and polynomial closure coefficients.

Fig. 2 is the general scheme for the FP\_ILM retrieval phase. The “extracted features” used in each case are algorithm dependent, for example for the GE\_LER retrieval we use the DOAS results and for the SO<sub>2</sub> layer height retrieval we use principal components.

4) Clarify what are effects of UV-absorbing aerosols (dust or smoke) on GE\_LER?

Absorbing aerosols can induce GE\_LER values lower than the actual surface LER. As already mentioned in Section 4.3, in the future we plan to use the S5P absorbing aerosol index for filtering the affected measurements.

5) Clarify that the neural network is trained on synthetic clear-sky spectra, but applied to the TROPKMI measurements over mixed, partly cloudy scenes (equation 5).

The GE\_LER retrieval is applied to all TROPOMI measurements. Equation 5 indicates only how we compute the effective surface height in case of cloud contamination.

6) Compare TROPOMI GE\_LER retrievals with the traditional LER retrievals at 340nm, where ozone absorption is negligible. Add TROPOMI simple LER<sub>340</sub> map to Figure 10.

We include a new Section 4.4 describing the comparison with GOME-2 and OMI LER.

7) Publicly release G3\_LER data set for community evaluation.

The retrieved GE\_LER and the G3\_LER used for each single TROPOMI ground pixel will be included in the operational S5P total ozone product. All operational S5P products are open and free available. We will discuss with ESA/EU the possibility of disseminating the G3\_LER total ozone daily maps in the same way as the operational S5P products.

## Technical comments

Table 2 is not mentioned in the text.

[reference added in Section 4.2](#)

P1, 12: with a significant[ly] lower spatial resolution . . .

[corrected](#)

13: satellite viewing [geometry] dependencies

[added](#)

P2,

1: are mayor [major] error sources – clarify that the surface reflectance has larger influence on boundary layer trace gases retrievals and much less on the mid-and upper-tropospheric constituent retrievals.

[corrected and clarification added.](#)

13: significant[ly] lower spatial resolution

[corrected](#)

18: (b) the effect of surface reflectance anisotropy [is]

[corrected](#)

20: Retrieval of [Lambertian] effective scene albedo has been used in total ozone algorithms from nadir and limb – add pioneering reference: Mateer et al., 1971.

[corrected. Reference to Mateer et al. added two sentences before.](#)

22: - add references to heritage TOMS ozone, e.g., Bhartia et al., 1996 McPeters, et al., 1998.

- and OMI ozone references, e.g., McPeters, et al., 2015 or Veefkind, et al., 2006.

[added references to Bhartia \(TOMS\) and McPeters \(OMI\)](#)

24: from other [higher spatial resolution] satellite sensors

[added](#)

28:” needed for computing LER from [and] BRDF may not be fully compatible” – need clarification: In Vasilkov et al., [2017] LER is calculated from the RT model simulated TOA radiance in a standard way, which is fully compatible with OMI cloud and NO<sub>2</sub> retrievals. However, MODIS BRDF product may use different RT assumptions.

[modified to “needed for computing MODIS BRDF may not be fully compatible”](#)

P3,

16: errors could be large and [multi-dimensional interpolations are] time consuming. .

modified to *“the interpolation/extrapolation in this multi-dimensional space are computational expensive, and the interpolation/extrapolation errors could be significant”*

21: During the last years we [Recently] we developed an approached called . . .

modified

22: applied for retrieving [ozone] profile shapes . . .

added

P4,

4, . . . the surface properties - clarify what properties? Did you use RTM with Lambertian surface for training or did you use RTM with BRDF model? Specify, which land/ocean BRDF model/dataset was used for training ?

clarification added *“Lambertian surface properties”*

15 resolution to resolve [absorbing] features

added

16 usually contains [hyperspectral] radiances at a high-dimensional space

added

17 . . .avoiding the effects of the curse of dimensionality ? – clarify

sentence deleted

27 Explain where does the GE\_LER information come from (i.e., equation (3))?

at the end of Section 2.1 (same page as equation (3)) it is already indicated that surface properties  $A_e$  are the source of the GE\_LER

P5,

19 . . . effective scene approximation - add reference ([Mateer et al., 1971, Coldewey-Egbers et al., 2005])

added

21 whereas a [clear-sky] LER is needed

added

22 GE\_LER retrieved under clear sky conditions – explain cloud masking algorithm  
explanation included

24, Fig 3 . . . based on the [GE\_]LER data from previous days – Clarify if the GE-LER map instrument and viewing geometry specific?

The sentence after this already explains that the G3\_LER map should include the viewing geometry dependencies. The GE\_LER is instrument specific as it is based on L1 measurements of a given instrument.

25-26 (BRDF) effects, as it is based on radiative transfer model simulations using the actual viewing geometry – clarify did you use RTM with Lambertian or BRDF surface? What surface BRDF model/dataset (if any) was used in creating training spectral dataset?

RTM with Lambertian surface is used, see also reply to comment P4/4.

P6,

2 fitting a polynomial of clear-sky LERs averaged as function of  $\theta$  . – Please, clarify: - sentence reformulated as follows: *“the dependency on the solar zenith angle can be characterized by fitting a polynomial (or exponential) function over clear-sky LERs sorted as function of  $\theta$ ”*

should BRDF function also depend on solar and azimuthal angles in addition to satellite view angle?

- Provide examples (add figure) of the clear sky LER( $\theta$ ) for land and water surfaces.

this explanation is added *“solar zenith angel dependencies can be ignored when combining GE\_LER data from Sun-synchronous satellites over the same position because the angle of sunlight upon the Earth's surface is consistently maintained. Likewise relative azimuth angle dependencies are negligible in the UV”*

17 synthetic UV spectra – clarify that spectra were simulated assuming Lambertian surface, no aerosols and no inelastic RRS effects.

see reply to General comment 1)

19 ozone [profile?] climatology  
added

24 Figure 4 shows the optical densities difference – clarify definition of the optical density and the OD difference. Explain why is Figure 4 necessary?

25 ... albedo of 0.05, 0.3, 0.6, and 0.9 [,which] correspond to water,.. – not clear how [ozone?]

optical density is related to the surface albedo?

clarification added *“optical densities of the DOAS polynomial in Equation (2)”*

*Fig. 4 nicely illustrate how the optical densities of the DOAS polynomial change for different conditions*

28 higher [longer?] wavelength.

corrected

P7,

1, Fig 4 . . . optical density increases when the viewing zenith angle decreases – please, explain. The ozone optical density is proportional to the slant column ozone amount, which should decrease when the viewing zenith angle decreases. . . . for all cases, the optical density increases along the wavelength region – Explain why is this important?

clarification added *“optical densities of the DOAS polynomial*

3 . . . is reorganized according to (3) – clarify the meaning of equation (3) an reorganization algorithm

sentence reformulated to *“The simulation results from (3) are reorganized by grouping as input the DOAS polynomial coefficients and ozone slant column, the viewing geometry, and surface height”*

5 . . . using a NN with a topology of 9-20-8-2-1, - provide reference to the NN software used and how the optimal topology has been selected?

see reply to [General comment 3b](#)

10, Fig.5 . . . represents the inverse function [of the synthetic dataset] in a very precise way – this does not guarantee similar accuracy when applied to the real satellite measurements.

we agree

Figure 6(a) title and color bar show “E\_LER” – change to GE\_LER

Figure 6(b) – explain cloud fraction stripes over Antarctica?

*The cloud stripes over Antarctica are an artefact of the S5P v1 cloud retrieval algorithm that is based on OMI cloud-free composites and scan angle corrections. The S5P v2 of the cloud algorithm solves this issue.*

20 In the case of clear-sky ( $\delta \tau_{IS}, \delta \tau'_{IS}, R \leq 0.05$ ) the GE\_LER represents the surface albedo – clarify if GE\_LER represents hemispherical albedo or directional BRDF ?

clarification added *“hemispherical surface albedo”*

25 the TROPOMI clear-sky GE\_LER and OMI LER climatology – Add comparison with the

OMI/TROPOMI simple LER at 340nm in Table 2.

26 summarized in Figure 7. - in Table 2?

We include a new Section 4.4 describing the comparison with GOME-2 and OMI LER.

P8,

1 . . . aggregating normalized [GE\_]LER from the couple of days. – these retrievals are obtained under different viewing geometries. - Couple of days may not be sufficient to obtain cloud-free observations over certain locations. - Explain how GE\_LER are normalized and what viewing geometry does the aggregated G3\_LER map correspond to?

sentence reformulated.

explanation added *“normalized to the central detector pixel (nadir)”*

10 . . . averaged as function of the viewing zenith angle. – BRDF depends also on solar zenith and relative solar azimuthal angles. Why is this dependence ignored?

see reply to P6, 2

Fig. 8 Why is sun-glint is not visible for the water surface GE\_LER and “hot spot” is not visible for the land GE\_LER ?

What would GE\_LER look like for a cloud-free sun-glint region?

as already explained in the second sentence of 4.3, measurements affected by sun-glint are not used in the G3\_LER

Fig. 9(a) – what viewing geometry does the aggregated G3\_LER map corresponds to? Reduce upper scale or use logarithmic scale to better show LER variability for snow-free regions.

nadir, see also reply to P8, 1

Clarify wavelength for the OMI climatological LER.

*“(335 nm)”* added

Fig 9 caption: the ma[j]or differences

corrected

Fig 10. Add comparison with the TROPOMI simple LER map at 340nm (negligible ozone absorption)

TROPOMI LER at 340 nm is not available

25 associated to [with] the coarse resolution

corrected

26 most important[ly]

corrected

p9,

5 what is even wors[e]

corrected

11 reduced from  $-2.53 \pm 2.46\%$  using OMI LER to  $0.78 \pm 3.49\%$  using TROPOMI G3\_LER - why did the standard deviation increase?

it was a typo, the correct value should be 2.49

P12,

11 Loyola, D., et al.: The near-real-time total ozone retrieval algorithm from TROPOMI onboard Sentinel-5 Precursor, Atmos.Meas. Tech. Discuss., in preparation, 2019. –provide complete citation

done

# Applying FP\_ILM to the retrieval of geometry-dependent effective Lambertian equivalent reflectivity (GE\_LER) ~~daily maps from~~ ~~to account for BRDF effects on~~ UVN satellite measurements ~~of trace gases, clouds and aerosols~~

5 Diego G. Loyola<sup>1</sup>, Jian Xu<sup>1</sup>, Klaus-Peter Heue<sup>1</sup>, Walter Zimmer<sup>1</sup>

<sup>1</sup>German Aerospace Centre (DLR), Remote Sensing Technology Institute, Oberpfaffenhofen, 82234 Wessling, Germany

Correspondence to: Diego Loyola ([Diego.Loyola@dlr.de](mailto:Diego.Loyola@dlr.de))

**Abstract.** The retrieval of trace gas, cloud and aerosol measurements from ultraviolet, visible and near-infrared (UVN) sensors requires precise information on ~~the~~ surface properties that are traditionally obtained from Lambertian equivalent reflectivity (LER) climatologies. The main drawbacks of using ~~such~~ LER climatologies for new satellite missions are (a) climatologies are typically based on previous missions with ~~a~~ significantly lower spatial resolutions, (b) they usually do not ~~fully take into~~ account ~~the fully for~~ satellite viewing geometry dependencies characterized by ~~the~~ bidirectional reflectance distribution function (BRDF) effects, and (c) climatologies may differ considerably from the actual surface conditions especially ~~under with~~ snow/ice ~~situations~~ scenarios.

In this paper we present a novel algorithm for the retrieval of geometry-dependent effective Lambertian equivalent reflectivity (GE\_LER) from UVN sensors; ~~the algorithm is~~ based on the full-physics inverse learning machine (FP\_ILM) retrieval. ~~The r~~Radiances are simulated using a radiative transfer model that takes into account the satellite viewing geometry and the inverse problem is solved using machine learning techniques to obtain the GE\_LER from satellite measurements.

20 The GE\_LER retrieval is optimized ~~not only for the~~ trace gas retrievals ~~employing using~~ the DOAS algorithm, ~~but also for~~ ~~and~~ the large amount of data ~~from existing and future of the new~~ atmospheric Sentinel satellite missions. The GE\_LER can either be ~~deployed used~~ directly for the computation of AMFs using the effective scene approximation or ~~it can be used to create~~ a global gapless geometry-dependent LER (G3\_LER) daily map ~~can be easily created~~ from the GE\_LER under clear-sky conditions for the computation of AMFs using the independent pixel approximation.

25 The ~~FP\_ILM~~ GE\_LER algorithm is applied to measurements of TROPOMI launched in October 2017 on board the EU/ESA Sentinel-5 Precursor (S5P) mission. The TROPOMI GE\_LER/G3\_LER results are compared with climatological OMI ~~and~~ [GOME-2](#) LER datasets and the advantages of using GE\_LER/G3\_LER are demonstrated for the retrieval of total ozone from TROPOMI.

## 6. Introduction

Lack of knowledge of the magnitude of ~~Uncertainties about the~~ surface reflectance and ~~the neglect of surface not accounting~~ ~~their~~-anisotropic ~~effects~~ ~~properties~~ are ~~the two~~ major error sources for the retrieval of trace gas, cloud and aerosol information from ultraviolet, visible and near-infrared (UVN) satellites measurements (Vasilkov et al., 2018; Lorente et al., 2018; Lin et al., 2014; Seidel et al., 2012; Zhou et al., 2010). ~~Surface reflectance has a stronger influence on the retrievals of~~ ~~boundary layer trace gases and aerosols than is the case for mid- and upper-tropospheric trace gas and cloud retrievals.~~ For example errors of 0.02 in the surface reflectivity may induce errors of 10%–20% in ~~retrieved~~ SO<sub>2</sub> column ~~amount~~ (Lee et al., 2009) and seasonal snow cover ~~could-can~~ change the retrieved NO<sub>2</sub> column by 20%–50% (O'Byrne et al., 2010) and the retrieved O<sub>3</sub> column by 5%–35% (Lerot et al., 2014).

~~The Lambertian Equivalent Reflectivity (LER) concept was first introduced for the BUV (Backscatter Ultra-Violet) total ozone retrievals (Mateer et al., 1971) and it was extended to retrievals of tropospheric ozone, NO<sub>2</sub>, SO<sub>2</sub> and other pollutants under partly cloudy conditions using the independent pixel approximation (Ahmad et al., 2004).~~ Traditionally, surface properties are obtained from ~~Lambertian equivalent reflectivity (LER)~~ climatologies and in the case of new missions ~~like such as~~ TROPOMI launched in October 2017 on board the EU/ESA Sentinel-5 Precursor (S5P) mission, ~~the~~ climatologies used at ~~the beginning of the~~ mission ~~start~~ are based on LER data from previous missions ~~like-such as~~ TOMS (Herman and Celarier, 1997), GOME (Koelemeijer et al., 2003), OMI (Kleipool et al., 2008), SCIAMACHY (Tilstra et al., 2017), and GOME-2 (Pflug et al., 2008).

The unprecedented spatial resolution of TROPOMI (~~3.5 x 5.5 km<sup>2</sup> currently and 3.5x7 km<sup>2</sup> for data before August 6<sup>th</sup> 2019~~) ~~has~~ clearly ~~showed-shown~~ the disadvantages of using LER climatologies based on previous missions with ~~a~~ significantly lower spatial resolution. ~~Indeed, The~~ initial ~~studies version~~ of the TROPOMI trace gas ~~retrieved~~ products ~~based on such LER~~ ~~using~~ climatologies ~~have exhibited show~~ flawed patterns related to the coarser resolution of the OMI LER climatology. A LER climatology based on TROPOMI measurements could solve this particular problem, but creating ~~such-a~~ new TROPOMI LER climatology will probably require at least two years of data. Furthermore, there are two ~~fundamental common~~ problems with typical LER climatologies: (a) the actual surface conditions of a satellite measurement may differ considerably from climatological values ~~like, as~~ for example ~~under-for~~ snow/ice ~~scenarios~~situations, and (b) the effect of surface reflectance anisotropy ~~are-is~~ usually not properly covered by the climatology.

Retrieval of ~~Lambertian~~ effective scene albedo has been used in total ozone algorithms from nadir and limb satellite sensors, ~~see for example Bhartia et al., 1996 and McPeters, et al., 2015.~~ The WFDOAS (Coldewey-Egbers et al., 2005) ~~algorithm approach~~ retrieves the effective LER at 377 nm, ~~while~~ the GODFIT (Lerot et al., 2010) and SAGE III (Raul and Taha, 2007) approaches ~~both~~ retrieve simultaneously ~~the effective LER and other parameters along~~ with ~~total~~ ozone ~~the effective LER and other parameters.~~

Another approach used for NO<sub>2</sub> and cloud retrievals ~~involved is~~ the computation of LER from bidirectional reflectance distribution function (BRDF) data obtained from other satellite sensors ~~with higher spatial resolution.~~ In a recent work

(Vasilkov et al., 2017), the BRDF data from MODIS is first resampled to the lower resolution of the OMI instrument, and then a geometry-dependent LER is computed using radiative transfer model simulations. Unfortunately MODIS BRDF data is available only from visible (VIS) wavelengths and rescaling the VIS BRDF (or LER) to UV is not straightforward. Furthermore, the radiative transfer (RT) model assumptions needed for computing ~~LER from MODIS BRDFs~~ may not be fully compatible with ~~the RT model~~ assumptions required for UV-based trace gas retrievals.

In this paper we present a novel algorithm to be used not only for the retrieval of geometry-dependent effective Lambertian equivalent reflectivity (GE\_LER) from UVN measurements but also for ~~and~~ the creation of global gapless geometry-dependent LER (G3\_LER) daily map based on using GE\_LER data obtained for under clear-sky conditions. The retrieved GE\_LER/ and G3\_LER ~~retrieval should represent the current surface conditions, while mitigating solves~~ the problems of using LER climatologies, and accounting for surface anisotropy effects in cloud, aerosol and trace gas retrievals, in a similar manner way as does the effective LER (Coldewey-Egbers et al., 2005) and the geometry-dependent LER (Qin et al., 2019). But in contrast to these approaches, the GE\_LER retrieval is performed in precisely exactly the same fitting windows used for the trace gas, cloud and aerosol retrievals themselves; furthermore our algorithm does not require external data sources such as from other sensors like BRDFs (land surfaces) or Chlorophyll and wind parameters (water surfaces).

First we describe in sSection 2 the full-physics inverse learning machine (FP\_ILM) technique used for the retrieval of GE\_LER from UVN measurements, and we demonstrate how it is optimized for ~~the~~ DOAS trace gas retrievals. Section 3 discusses describes the creation of global gapless geometry-dependent LER (G3\_LER) daily maps using the retrieved GE\_LER under for clear-sky conditions. In section 4 we apply the GE\_LER algorithms to S5P measurements, first and then ~~we compare the~~ TROPOMI G3\_LER results with climatological OMI and GOME-2 LER data, and secondly. ~~Finally in~~ Section 5 we demonstrate the advantages of using GE\_LER/G3\_LER for the retrieval of total ozone from TROPOMI, and ~~in~~ Section 56 we discuss future work.

## 7. The FP\_ILM algorithm for the GE\_LER retrieval

Trace gas, cloud and aerosol retrievals from UVN measurements rely on complex radiative transfer model (RTM) simulations. ~~The~~ RTM calculations are computationally expensive and therefore not well suited for processing massive the ~~big~~ data from the new generation of atmospheric composition Sentinel missions. A classical approach for speeding up ~~the~~ RTM performance simulations is to use look-up tables (LUTs), ~~but they require significant amount of memory and what is more important the interpolation/extrapolation errors could be large and time consuming.~~ The main drawbacks of LUTs with high dimensionality (common in atmospheric composition retrievals) are that the memory requirements increase exponentially with the number of input dimensions, the interpolation/extrapolation in this multi-dimensional space are computationally expensive, and interpolation/extrapolation errors can be significant. To ~~solve avoid~~ these LUT issues, the DLR team has developed during the last two decades machine learning techniques for the optimal generation of RTM samples (Loyola et al., 2016) and the accurate parameterizationing of RTM simulations using artificial neural networks

(NN). These algorithms are being used for the operational processing of GOME-2 (Loyola et al., 2010) and now TROPOMI (Loyola et al., 2018) data.

Machine learning can be used not only for forward problems (~~like such as~~ the parameterization of RTM simulations), but also for solving inverse problems, see for example (Loyola et al., 2016). ~~Recently During the last years~~ we have developed an approach called the “full-physics inverse learning machine” (FP\_ILM) technique; ~~this has been applied that was~~ successfully ~~applied~~ for retrieving ozone profile shapes from GOME-2 (Xu et al., 2017) and retrieving SO<sub>2</sub> layer height from GOME-2 (Efremenko et al., 2017) and TROPOMI (Hedelt et al., 2019).

**Figure 1** ~~presents shows~~ a flow diagram of the different steps of the FP\_ILM algorithm and the following subsections describe in more detail how FP\_ILM is ~~tailored applied~~ for the retrieval of GE\_LER.

## 7.1. Forward Model

The forward model segment has two components: first a radiative transfer model (RTM) that computes ~~the~~ spectral intensity as a function of the solar and viewing geometry, atmospheric components and Lambertian surface properties; and second a sensor model that transforms the RTM intensities spectra to simulated spectra using sensor information such as ~~like~~ the instrument spectral response function and ~~the instrument~~ signal to noise ratio.

The forward model  $F$  ~~can be used to compute will~~ simulated spectral radiances  $R_{sim}$  for a given wavelength  $\lambda$  according to as

$$R_{sim}(\lambda) \pm \varepsilon_R = F(\lambda, \Theta, \Omega, A_e, Z_e) \quad (6)$$

where  $\varepsilon_R$  denotes the expected instrument error,  $\Theta$  is the light path geometry (solar and satellite zenith and azimuth angles),  $\Omega$  are the atmospheric composition components, and the surface properties denoted by  $A_e$  for the geometry-dependent effective Lambertian equivalent reflectivity (GE\_LER) and  $Z_e$  for the effective surface pressure height.

## 7.2. Smart Sampling

Traditionally, training data are created at uniformly distributed fixed intervals for each input variable; as a consequence, the training samples are grouped around the node points and poor coverage of the multidimensional input space is the result. Deterministic sampling methods provide a more uniform distribution of the training data covering the entire space of each input variable.

A key element of FP\_ILM is the creation of a training data set that ~~extensively~~ covers extensively the multidimensional space of the forward problem and at the same time minimizes the computational expensive calls to the radiative transfer model. We use the smart sampling techniques (Loyola et al., 2016) for creating a dataset of samples  $\{\Theta, \Omega, A_e, Z_e\}$  that fully represent the expected viewing and geophysical conditions of the problem at hand. For this work we select a Halton sequence that uses prime numbers for creating sample points in each input dimension and a RTM that computes the corresponding simulated radiances.

As ~~indicated shown~~ in **Figure 1**, the smart sampling and forward module calls are iterated in a loop until the multi-dimensional integral of the output samples dataset  $\{R_{sim}(\lambda) \pm \varepsilon_R\}$  converges. This technique allows us to determine the minimum number of samples needed to properly cover the output space; see (Loyola et al., 2016) for more details.

### 7.3. Feature Extraction

5 Retrieval of trace gas, cloud and aerosol concentrations from UVN sensors requires spectrometers with sufficiently detailed spectral resolution to resolve absorbing features in the electromagnetic spectrum. ~~Therefore the fitting window used for the retrieval of a trace gas usually contains requires hyperspectral radiances at for~~ a high-dimensional space (tens to hundreds of wavelengths). Machine learning techniques perform best with low-dimensional datasets ~~by avoiding the effects of the curse of dimensionality~~.

10 Feature extraction is a mapping function that transforms a dataset from a high- to a low-dimensional space by the removing of redundant information and noise. In previous FP\_ILM applications (Loyola et al., 2006; Xu et al., 2017) we used principal component analysis for the feature extraction. ~~However for the GE\_LER retrieval we take advantage of the DOAS fitting results model~~

$$R_{sim}(\lambda) = -\sum_g N_{s,g}(\Theta) \cdot \sigma_g(\lambda) - pP(\lambda) \quad (7)$$

15 wherewith  $N_{s,g}(\Theta)$  is the effective slant column density of gas  $g$  for ~~the~~ light path geometry  $\Theta$ ,  $\sigma_g(\lambda)$  the associated trace gas absorption cross-section ~~for at~~ wavelength  $\lambda$ , and  $pP(\lambda)$  ~~the an~~ external closure polynomial.

The feature extraction step ~~comprises ansists in~~ application of the DOAS fit to the simulated radiances. Combining (1) and (2) for a given fitting window  $\Lambda$  we obtain the following approximation with simulated datasets that represent ~~ing~~ the forward problem

20 
$$\{N_{s,g}(\Theta), P(\Lambda)\} \cong \{F(\Theta, A_e(\Lambda), Z_e)\} \quad (8)$$

where  $A_e(\Lambda)$  is the wavelength independent GE\_LER for the particular DOAS fitting window.

### 7.4. Machine Learning

Machine learning approximates a function that is represented by input/output datasets ~~by means of using either~~ linear or non-linear regression algorithms. In this paper we use artificial neural networks (NN) to learn the non-linear inverse problem by ~~reorganizing the datasets from (3) to represent the inverse problem~~:

$$\{A_e(\Lambda)\} \cong \{F_{NN}^{-1}(pP(\Lambda), N_{s,g}, \Theta, Z_e)\} \quad (9)$$

In other words, a neural network will ~~solves~~ the inverse problem and retrieves the GE\_LER as function of the DOAS closure polynomial, the DOAS fitted effective slant column density, the viewing geometry and the effective surface height pressure.

The inverse operator itself is the collection of ~~are~~ the weights and biases of the neural network approximating  $F_{NN}^{-1}$ .

## 7.5. GE\_LER Retrieval

Obtaining the inverse operator is very time consuming mainly due to the relatively large amount of RTM simulations needed to properly ~~characterize represent~~ the forward problem. Finding a neural network (NN) topology that learns the inverse function with ~~minimum a small~~ error is also computationally intensive. ~~However, But~~ all these steps are carried out done offline and need to be done only once for a given sensor and trace gas fitting window.

Figure 2 shows the flow diagram for applying the FP\_ILM to satellite measurements. There is no additional extra computation needed for the feature extraction part, as we are using ~~the~~ results from the DOAS fitting; also, application and the application of the NN to retrieved GE\_LER is extremely-very fast as it only involves simple matrix multiplications.

The ~~extremely~~ exceptionally fast retrieval using the FP\_ILM is a crucial advantage for the operational near-real-time processing of the Big Data from ~~the~~ current and future atmospheric composition Sentinel missions.

## 8. Global Gapless Geometry-dependent (G3) LER Daily Map

~~The e~~Conversion of ~~the~~ DOAS effective slant column amounts to a ~~geometry-~~independent total column requires the calculation of air mass factors (AMF) calculated using either the effective scene approximation (Mateer et al., 1971; Coldewey-Egbers et al., 2005) or the independent pixel approximation (e.g. Loyola et al., 2011). The retrieved GE\_LER can be used directly for ~~the AMF~~ computation of AMFs using based on the effective scene approximation; ~~whereas a clear-sky~~ LER is needed for ~~the computation of~~ AMFs using calculated with the independent pixel approximation.

A global gapless geometry-dependent LER (G3\_LER) daily map can be easily created from GE\_LER values retrieved under clear-sky conditions. In the case of S5P, a clear-sky situation is established not only with the operational cloud properties retrieved from TROPOMI (Loyola et al., 2018) but also with the VIIRS/SNPP (Visible Infrared Imaging Radiometer Suite sensor, on board the Suomi National Polar-orbiting Partnership satellite) cloud mask regridded to the TROPOMI spatial resolution (R. Siddans, 2016). Note that S5P and SNPP fly in loose formation, with the S5P orbit trailing 3 to 5 minutes behind SNPP.

The G3\_LER map for a given day is created by merging the clear-sky GE\_LER data from the same day with the G3\_LER map based on the GE\_LER data from previous days, see Figure 3. The spatial resolution of the G3 LER maps for TROPOMI is 0.1° latitude and 0.1° longitude, and global maps can in general be derived by combining data from a single month. Two to three months of data are needed only for regions with persistent cloud cover such as the Intertropical Convergence Zone (ITCZ).

It is important to note that the GE\_LER determination incorporates takes into account the bidirectional reflectance distribution function (BRDF) effects, ~~as since~~ it is based on radiative transfer model simulations using the actual viewing geometry. ~~But w~~When combining GE\_LER data their BRDF dependencies  $\rho(\lambda, \theta, \psi)$  as function of the wavelength in the

fitting window  $\Lambda$ , the viewing zenith angle  $\theta$ , and the surface types  $\psi$  must be considered. In contrast, solar zenith angle dependencies can be ignored when combining GE\_LER data from sun-synchronous satellites over the same location, because the angle of sunlight at the Earth's surface is consistently maintained. Likewise relative azimuth angle dependencies are negligible in the UV. The  $\rho(\Lambda, \theta, \psi)$  dependencies ~~function~~ can be ~~easily~~ obtained separately for different fitting windows  $\Lambda$  (in the UV, VIS and NIR spectral region), for different surface types  $\psi$  (e.g. land, water, snow/ice) and various time periods (e.g. monthly); any dependency on viewing zenith angle can be characterized by fitting a polynomial (or exponential) function of over clear-sky LERs ~~averaged-sorted~~ as function of  $\theta$ .

The G3\_LER daily map ~~comprises the contains~~ normalized LER, i.e. the GE\_LER retrieved under clear-sky conditions divided by the fitted BRDF dependency, as well as the multiplicative factors  $\rho(\theta)$  needed to compute the geometry-dependent LER as a function of the actual satellite viewing zenith angle  $\theta$ .

It is necessary to aggregate normalized LER retrievals over several days (between one to four weeks depending on cloudiness) in order to obtain a global gapless map. In contrast to LER climatologies, the G3\_LER map represents ~~the~~ actual surface properties as it is updated on a daily basis. The only exceptions are cases of sudden snow fall combined with significant cloudiness.

## 9. GE\_LER and G3\_LER from TROPOMI/S5P 325-335 nm

In this section, we apply the ~~The~~ GE\_LER and G3\_LER algorithms described in the previous sections ~~are applied~~ to measurements of TROPOMI/S5P in the total ozone wavelength region. The S5P operational near-real-time total ozone products (Loyola et al., 2019) are based on the DOAS algorithm with using the fitting window ~~of~~ 325-335 nm. First we discuss aspects of the training process.

### 9.1. ~~FP\_HLM~~ GE\_LER Training

The training dataset is based on spectra simulated by the Vector Linearized Discrete Ordinate Radiative Transfer (VLIDORT) model (Spurr, 2016). The RTM inputs are ozone concentration profiles, Lambertian surface albedo, surface ~~height~~ pressure and the ~~viewing geometry~~ solar and viewing angles. The smart-sampling technique (Loyola et al., 2016) was used to create more than  $2 \times 10^5$  synthetic UV spectra for the using ozone profile, viewing geometry and surface parameters in the ranges listed in Table 1. We use the Bodeker et al., (2013) ozone profile climatology for representing the stratospheric ozone in conjunction ~~ozone database merged~~ with the McPeters/Labow (Labow et al., 2015) ~~ozone~~ climatology ~~for an optimal representation of the ozone vertical distribution in the stratosphere and lower tropospheric ozone.~~

Synthetic TROPOMI/S5P-like measurements are created by convolving these RTM radiances with applying the instrument slit function ~~to the RTM simulated radiances~~ and adding a Gaussian instrument noise with a signal-to-noise ratio of 300 representative of TROPOMI band 3, see Kleipool et al., 2018.

The DOAS fitting is applied to these simulated S5P radiances using the same DOAS settings as in the operational S5P retrieval including a cubic external-closure polynomial resulting in a dataset of ozone slant columns and associated the polynomial coefficients.

Figure 4 shows the optical densities difference of the DOAS polynomial ( $p(\lambda)$  in Equation (2)) for three scenarios: In panel (a) these are given as functions of ~~with respect to~~ four typical values of surface albedo of 0.05, 0.3, 0.6, and 0.9 which correspond to water, land, melted snow/ice-covered and fresh snow/ice-covered regions. The largest absolute value of the optical density corresponds to the highest largest surface albedo; ~~the~~ optical densities for the four albedos do not differ significantly at ~~the~~ lower wavelengths, while the differences are more significant increase at the higher longer wavelengths. In panel (b) optical densities of the DOAS polynomial are shown with respect to three total ozone columns of 150 DU, 300 DU, and 500 DU; ~~the optical density increases gradually along the selected wavelength region,~~ the absolute value of the optical density increases when the total ozone column increases. Finally in panel (c) densities are plotted for ~~with respect to~~ three viewing zenith angles of 50°, 30°, 10°; the absolute value of the optical density increases with decreasing ~~when the~~ viewing zenith angle ~~decreases~~. For all cases, ~~the~~ optical density increases along the with wavelength region.

The ~~input and output of the~~ simulation results from (3) are reorganized according to (3) and by grouping the DOAS polynomial coefficients, ozone slant column, the viewing geometries, and surface heights as inputs to the neural network. A feedforward neural network (the neurons are grouped in layers) is trained to learn the inverse function (retrieval of surface albedo) using 70% of the simulations for training, 15% for testing and 15% for validation. Different NN topologies were tested using one, two, and three hidden layers; ~~t~~he best results are obtained using a NN with a topology of 9-20-8-2-1, which is 9 neurons in the input layer, three hidden layers with the given number of neurons, and one neuron on the output layer.

In Figure 5, we depict the GE\_LER retrieval errors as function of the different input parameters calculated using the validation dataset (i.e. part of the dataset not used for ~~the~~ NN training) are depicted in Figure 5; the x-axes are divided into bins and the mean and standard deviation (red bars) are calculated for each bin. The differences between the *true* and retrieved GE\_LER are very small with a mean and standard deviation of only  $0.0016 \pm 0.0018$ . These results demonstrate that the NN represents the inverse function in a very accurate manner ~~precise way~~.

The Ring effect (filling in of Fraunhofer and telluric spectral signatures through inelastic rotational-Raman scattering by air molecules) is a significant spectral interference in DOAS total ozone fitting in the 325-335 nm window. We tested its impact for the GE\_LER training by adding filling-in corrections obtained with the LIDORT-RRS model (Spurr et al., 2008) to the VLIDORT simulations. We found that the Ring-effect impact on GE\_LER retrieval in the ozone fitting window is not significant. Indeed, the mean difference in GE\_LER retrievals with and without the inclusion of LIDORT-RSS corrections is in the range of  $5e-5$  for  $SZA < 75^\circ$  and  $3.5e-4$  for larger SZA.

The BRDF effects on the ozone fitting window are well modelled using the GE\_LER approximation, the difference in the total ozone retrieved using VLIDORT with and without the BRDF supplement is in the order of 0.5 DU or 0.2%.

## 9.2. FP\_ILM-GE\_LER Retrieval

The neural network trained with the inverse function is applied to TROPOMI/S5P measurements. The inputs are the DOAS fitted polynomial coefficients and ozone slant column, the solar and viewing zenith angles, the relative azimuth angle, and the effective surface heightpressure  $Z_e$  computed in the independent-pixel approximation as

$$Z_e = (1 - f_c)Z_s + f_c Z_c \quad (10)$$

where  $f_c$  is the cloud fraction,  $Z_s$  the surface heightpressure, and  $Z_c$  the cloud heightpressure. The S5P cloud properties are obtained from the operational TROPOMI cloud products using the OCRA and ROCINN algorithms (Lutz et al., 2016; Loyola et al., 2018)-algorithms.

It is known that version 1 of the TROPOMI Level 1 product has small deficiencies in the UV band (Rozemeijer and Kleipool, 2019); therefore a “soft” correction based on comparisons with OMPS radiances is applied to the S5P radiances. It is expected that these issues will be solved for version 2 of the TROPOMI Level 1 product, obviating the need for this soft correction.

~~The~~ TROPOMI/S5P GE\_LER results for the total ozone fitting window (325-335 nm) for April 10<sup>th</sup>, 2018 are shown in Figure 6. ~~As~~ expected the GE\_LER field shows the same patterns as the clouds field for that day. ~~In the case of~~ For clear-sky conditions ( $f_c \leq 0.05$ ) the GE\_LER represents the hemispherical surface albedo ~~and, while~~ for ~~the~~ cloudy scenarios ~~eases~~ ( $f_c \geq 0.95$ ) ~~the~~ GE\_LER represents the cloud albedo. Figure 7 shows ~~the~~ histograms of the differences between the TROPOMI clear-sky GE\_LER and the OMI LER climatology (Kleipool et al., 2008) and also the differences between the cloudy TROPOMI GE\_LER and the cloud albedo from the operational cloud product retrieved with ROCINN\_CRB (Loyola et al., 2018). The second mode around 0.5 in the histogram ~~for the snow/ice eases~~ indicates snow- or ice-cover conditions scenarios in TROPOMI data that are ~~not well~~ poorly represented ~~in with~~ the OMI LER climatology. The comparison between S5P GE\_LER and the GOME-2 and OMI climatologies is discussed in more detail in Section 4.4.

~~The m~~Mean differences for the clear-sky and cloudy cases as a function of the surface type are summarized in Table 2 ~~and~~ Figure 7, with the relatively larger offsets and spreads ~~are~~ mainly due to the differences et in spectral regions betweeneovered by GE\_LER retrieved for the total ozone fitting window in the UV (325–335 nm) and the cloud properties retrieved with ROCINN\_CRB from the O<sub>2</sub>oxygen-A-bBand in the NIR (758–771 nm).

## 9.3. G3\_LER Daily Map

The TROPOMI G3\_LER map for a given day is created by regridding (using at resolution 0.1° x 0.1°-resolution) ~~and~~ aggregating normalized LER from the couple of days the clear-sky LER data from the same day with the G3\_LER map based

on LER data from previous days. The ~~FP\_HLM~~-LERs are obtained from the S5P GE\_LER retrievals under clear-sky conditions. In this version of the TROPOMI G3\_LER map we use the S5P OCRA and the VIIRS/SNPP (flying in constellation with S5P) cloud fractions  $f_c$  for identifying clear-sky measurements, ~~more concretely, we use the measurements with ( $f_c \leq 0.05$  is the criterion here).~~ In the future we plan to additionally use the S5P absorbing aerosol index product ~~and the regrided VIIRS/SNPP (flying in constellation with S5P)~~ for an even more stringent cloud/aerosol screening.

~~The~~ Ground pixels affected by sun glint ~~as well as the pixels influenced by~~ and solar eclipse are removed according to using the corresponding flags available in the S5P total ozone product (Pedernana et al., 2018). The remaining ~~FP\_HLM~~-LERs from a given day replace the corresponding grid points of the G3\_LER map from the previous day. Time information (orbit number) of the LER used in each grid cell is included in the G3\_LER maps.

The BRDF dependencies  $\rho(\theta)$  are calculated by fitting a polynomial to the TROPOMI LER data normalized to the central detector pixel (nadir viewing) and averaged as function of the viewing zenith angle. Three different surface types are considered: land, water and snow/ice. Figure 8 shows the BRDF dependencies calculated with normalized TROPOMI/S5P data from January, April, July and October 2018. ~~For~~ The surface classification we use is based on the ~~Land/W~~ water mask and the snow/ice flags available in from the S5P total ozone product (Pedernana et al., 2018). Note that these surface types are appropriate to BRDF effects in the UV ozone fitting window; other trace gases retrievals (such as NO<sub>2</sub> in the visible spectrum) will require different land cover types (e.g. water, snow/ice, urban, paddy, crop, deciduous forest, evergreen forest) to properly model BRDF effects; see Noguchi et al., 2014.

Figure 9 shows the TROPOMI/S5P G3\_LER daily map ~~corresponding to~~ April 30<sup>th</sup>, 2018, ~~and plus~~ a comparison ~~to with~~ the OMI LER climatology for the month of April. The OMI LER climatology is based on 3 years of data (2004 to 2007) whereas the TROPOMI G3\_LER ~~contains data of is based~~ only a few weeks of data. The main advantages of the TROPOMI G3\_LER daily map compared to climatology are first that it better represents ~~the~~ current surface conditions ~~like such as~~ snow/ice contamination; second that it takes into accounts for the BRDF effects; and third that it has ~~improved a better~~ spatial resolution (0.1°).

#### 9.4. G3\_LER comparison with OMI and GOME-2 LER

In this section we compare TROPOMI G3\_LER with climatology LER from OMI (Kleipool et al., 2008) and GOME-2 (Tilstra et al., 2017). Since TROPOMI G3\_LER is retrieved with fitting window 325 to 335 nm, we chose 335 nm LER values from the two climatologies. For GOME\_2 there is no shorter wavelength available in the published dataset, and for the OMI climatology use of the 328 nm is not recommended (Kleipool et al., 2010). In the following the instrument names will act as synonym for the respective albedo data sets. The three albedo datasets have different time and horizontal resolutions: OMI covers four years with grid resolution 0.5°, GOME: covers six years with grid resolution 0.25°, and TROPOMI covers only one year with a grid of 0.1°.

The histograms in Figure 10 show the differences between the TROPOMI, OMI and GOME-2 albedo maps for three different surface types land water and snow/ice. A grid cell is assumed to contain snow/ice if the albedo of all three instruments is above 0.7, and the latitude is outside the  $\pm 60^\circ$  range. For the snow- and ice-free observations over land and sea, the latitude range was restricted to  $\pm 40^\circ$ . In general the three data sets agree quite well. Over land and water the mean differences are lower than 0.03 and the distributions are small (standard deviation around 0.04). The histograms with S5P over land have tails towards higher values of up to 0.1 indicating that for some areas S5P data overestimate the albedo. According to the corresponding world maps (Figure 11) this occurs mainly over rain forests in Brazil, central Africa or Indonesia, where the TROPOMI data might be affected by residual cloud contamination. Note that for TROPOMI we have only one year of data compared to the multi-years for OMI and GOME-2

Over snow and ice larger deviations are found between OMI and GOME-2 LERs and between TROPOMI G3\_LER and the climatological OMI/GOME-2 LERs. We conclude that the historical climatologies from OMI and GOME-2 do not properly represent actual snow/ice conditions observed in 2018/2019.

#### 9.4.9.5. Usage of TROPOMI/S5P G3\_LER for the Total Ozone retrieval

The near-real-time S5P total ozone product is based on an iterative DOAS/AMF algorithm (Loyola et al., 2019) and the current operational version (1.1.57) uses the OMI LER climatology (Kleipool et al., 2008). The median bias between near-real-time total ozone from S5P and reference data from Brewer, Dobson, and SAOZ sites is of the order of +1% (Verhoelst et al., 2018; Garane et al., 2019).

S5P near-real-time ozone agrees well with the Copernicus Atmosphere Monitoring Service (CAMS) analysis with the exception of some anomalies at high latitudes (Inness et al., 2019). Those anomalies are associated ~~to~~ with the coarse resolution of the OMI LER climatology and most importantly, with the differences between the climatological LER values and the actual surface conditions (mainly like snow/ice).

When we replace the OMI LER climatology with the TROPOMI G3\_LER daily maps, and the resulting total ozone field is significantly smoother and has significantly fewer with far less outliers. Figure 12 shows the TROPOMI/S5P surface albedo and total ozone retrievals from April 1<sup>st</sup>, 2018 around the Bering Strait which separates Russia and Alaska. The TROPOMI G3\_LER daily map agrees very well with the surface types apparent visible in the corresponding VIIRS/SNPP images (S5P flies only 3-5 minutes behind SNPP) including the water surface along the coast lines of the shores of the Chukchi Sea in Russia, and the Sarichef Island in to the north of Alaska and the Seward Peninsula in south of Alaska. These coastal water surfaces along the coast as well as the open water of the Bering Sea are not properly well represented in the OMI LER climatology, which indicates that shows snow/ice cover for these regions sea areas. Similarly Likewise, the OMI LER climatology (erroneously) shows no snow/ice cover in the Yukon-Koyukuk Census Area in Alaska. The coarse spatial resolution of the OMI LER climatology is clearly visible in the total ozone field, and in addition, incorrect what is even

~~worst the wrong~~ snow/ice ~~assignments values~~ in the OMI LER climatology induce large errors on the retrieved total ozone with differences between  $-10\%$  and  $+15\%$ .

Moreover, ~~the~~ agreement of the S5P total ozone with the CAMS assimilation at high latitudes is significantly better ~~than that for the LER climatologies, as seen in, see~~ Figure 13. ~~The m~~ Mean differences between total ozone from S5P and CAMS for the complete month of April 2018 are summarized in Table 3. The agreement with CAMS improves considerably ~~in at~~ all latitude ~~es~~ ~~inal~~ ~~regions~~: ~~the~~ differences in the total ozone ~~in for~~ the region  $[80^{\circ}\text{S}-60^{\circ}\text{S}]$  ~~is are~~ reduced from  $-2.5361 \pm 2.4622\%$  using OMI LER to  $0.784 \pm 23.493\%$  using TROPOMI G3\_LER, ~~in the region for~~  $[60^{\circ}\text{S}-50^{\circ}\text{N}]$  ~~the difference remains at the same level with a small increase~~ ~~is reduced~~ from  $0.253 \pm 1.174\%$  to  $-0.1238 \pm 1.213\%$ , in the region  $[50^{\circ}\text{N}-70^{\circ}\text{N}]$  is reduced from  $1.214 \pm 2.465\%$  to  $-0.0179 \pm 21.0298\%$  and finally ~~in the region for~~  $[70^{\circ}\text{N}-90^{\circ}\text{N}]$  ~~the difference~~ is ~~reduced from~~  $-1.0041 \pm 2.58\%$  ~~compared~~ to  $-01.135 \pm 2.645\%$ .

## 10. Conclusions

We have developed a novel algorithm for the accurate and fast retrieval of geometry-dependent effective Lambertian equivalent reflectivity (GE\_LER) from UVN sensors based on the full-physics inverse learning machine (FP\_ILM) technique. The main inputs to the GE\_LER retrieval are the DOAS fitting polynomial ~~coefficients~~ and ~~the~~ fitted trace gas slant column ~~amounts~~, as well as the satellite viewing geometry. The inversion problem is solved using neuronal networks trained with radiative transfer model simulations based on the same kind of RTM and settings used for the AMF calculations.

A global gapless geometry-dependent LER (G3\_LER) daily map can be ~~easily~~ created from the GE\_LER retrievals under clear-sky conditions. ~~The G3\_LER daily maps better characterize current surface; in particular they minimize errors induced by the LER climatologies through inaccurate representation of snow/ice scenarios.~~ Both GE\_LER and G3\_LER ~~take into~~ account ~~the for~~ satellite viewing dependencies ~~which are~~ ~~characteristiczed~~ ~~by the~~ ~~bidirectional~~ ~~reflectance~~ ~~distribution~~ ~~function~~ ~~(of~~ BRDF) effects.

GE\_LER is retrieved from each single ground pixel using the same spectrum and DOAS/AMF settings as ~~those employed for the~~ trace gas retrievals, and ~~GE\_LER is~~ therefore ~~it is~~ fully consistent with the trace gas retrieval ~~itself~~. ~~This is~~ in contrast to LER products based on data from other satellites or LER data ~~derived~~ from the same satellite but using different fitting ~~window~~ or RTM settings. G3\_LER maps are updated on a daily basis using the ~~clear-sky~~ GE\_LER ~~under clear-sky conditions from for~~ that day, and ~~they are evidently therefore it is clearly~~ superior to LER climatologies that fail to represent ~~the~~ actual surface conditions ~~like snow/ice~~.

We have applied the FP\_ILM ~~algorithm to retrieve~~ GE\_LER ~~from TROPOMI for the 325-335 nm fitting window and~~ ~~thereby generate daily~~ G3\_LER maps that are used to retrieve the S5P total ozone, ~~and showed that the S5P~~ total ozone retrievals ~~based on using this novel product is~~ TROPOMI G3\_LER daily maps are clearly substantially superior to those

~~one created using the~~based on OMI\_LER climatology. The ozone fields are not only ~~much more~~smoother, but also the differences compared to the total ozone from CAMS in April 2018 is reduced from  $-2.53 \pm 2.46\%$  to  $0.78 \pm 3.49\%$  in the latitudinal region [80°S-60°S]. ~~Large errors~~in the S5P total ozone between  $-10\%$  and  $+15\%$  induced by snow/ice misrepresentations in the OMI\_LER climatology are removed using with the FP\_ILM GE\_LER/G3\_LER TROPOMI products.

5 ~~FP\_ILM~~ GE\_LER can be applied to any trace gas, cloud and aerosol product retrieved in the UVN and is fully compatible with the DOAS/AMF settings used for the trace gas retrievals. GE\_LER and G3\_LER can be used as inputs for computing AMFs, either with based on the effective scene assumption approximation or the independent pixel approximation respectively. In this paper we demonstrated their effectiveness for improving the quality of TROPOMI ~~the total ozone from TROPOMI~~; in the near future we will plan to extend GE\_LER/G3\_LER to ~~the fitting windows of for~~ the S5P operational  
10 UVN cloud product (Loyola et al., 2018), ~~and the~~ UV/VIS trace gases NO<sub>2</sub> (van Geffen et al., 2018), SO<sub>2</sub> (Theys et al., 2017), HCHO (De Smedt et al., 2018) as well as to fitting windows for S5P research products ~~like such as H<sub>2</sub>O, BrO, OCIO, CHOCHO~~ and aerosol optical depth.

The GE\_LER retrieval is accurate and extremely very fast and is therefore well suited for the (near-real-time) processing of ~~the huge amount of massive~~ data ~~of from~~ the atmospheric Sentinel satellite missions. We plan to apply the FP\_ILM  
15 GE\_LER/G3\_LER retrieval to the future Copernicus Sentinel-5 mission that (like Sentinel-5P) tracks along will follow a sun-synchronous polar orbit. Furthermore, we plan to assess the suitability of ~~FP\_ILM~~ GE\_LER to capture the diurnal LER dependencies on the sun-satellite geometry of the future UVN geostationary missions Sentinel-4, TEMPO and GMES.

## Acknowledgements

20 Special thanks to Robert Spurr for long-standing LIDORT support and editorial help. We thank the three reviewers for their insightful comments. This paper contains modified Copernicus Sentinel data processed by DLR. Thanks to EU/ESA/KNMI/DLR for providing the TROPOMI/S5P Level 1 products and NASA Worldview for the VIIRS/SNPP images used in this paper. We hereby acknowledge financial support from DLR ~~programmatische~~ (S5P KTR 2472046) for the development of TROPOMI retrieval algorithms.

## References

Ahmad, Z., Bhartia P. K., Krotkov N., Spectral properties of backscattered UV radiation in cloudy atmospheres, J. Geophys. Res. Atmos., 109, D01201, <https://doi.org/10.1029/2003JD003395>, 2004.

- Bhartia, P. K., McPeters, R. D., Mateer, C. L., Flynn, L. E., and Wellemeyer, C.: Algorithm for the estimation of vertical ozone profiles from the backscattered ultraviolet technique, *J. Geophys. Res.*, 101(D13), 18793–18806, <https://doi.org/10.1029/96JD01165>, 1996.
- 5 Bodeker, G. E., Hassler, B., Young, P. J., and Portmann, R. W.: A vertically resolved, global, gap-free ozone database for assessing or constraining global climate model simulations, *Earth Syst. Sci. Data*, 5/1, 31–43, 2013.
- Coldewey-Egbers, M., Weber, M., Lamsal, L. N., de Beek, R., Buchwitz, M., and Burrows, J. P.: Total ozone retrieval from GOME UV spectral data using the weighting function DOAS approach, *Atmos. Chem. Phys.*, 5, 1015–1025, <https://doi.org/10.5194/acp-5-1015-2005>, 2005.
- 10 Efremenko, D. S., Loyola R., D. G., Hedelt, P., and Spurr, R. J. D.: Volcanic SO<sub>2</sub> plume height retrieval from UV sensors using a full-physics inverse learning machine algorithm, *International Journal of Remote Sensing*, 38, 1–27, <https://doi.org/10.1080/01431161.2017.1348644>, 2017.
- 15 Garane, K., Koukouli, M.-E., Verhoelst, T., Lerot, C., Heue, K.-P., Fioletov, V., Balis, D., Bais, A., Bazureau, A., Dehn, A., Goutail, F., Granville, J., Griffin, D., Hubert, D., Keppens, A., Lambert, J.-C., Loyola, D., McLinden, C., Pazmino, A., Pommereau, J.-P., Redondas, A., Romahn, F., Valks, P., Van Roozendaal, M., Xu, J., Zehner, C., Zerefos, C., and Zimmer, W. et al.: TROPOMI/S5p total ozone column data: global ground-based validation and consistency with other satellite missions, *Atmos. Meas. Tech. Discuss.*, 12, 5263–5287, <https://doi.org/10.5194/amt-12-5263-2019> in preparation, 2019
- van Geffen, J. H. G. M., Eskes, H. J., Boersma, K. F., Maasakkers, J. D. and Veeffkind, J. P.: TROPOMI ATBD of the total and tropospheric NO<sub>2</sub> data products, S5P-KNMI-L2-0005-RP available at: <https://sentinel.esa.int/web/sentinel/technical-guides/sentinel-5p/products-algorithms> and <http://www.tropomi.eu/documents/level-2-products>, 2018.
- 20 Hedelt, P., Efremenko D.S., Loyola D.G., Spurr, R., and ~~Clarisse Lieven~~: Sulfur dioxide SO<sub>2</sub>-Layer Height retrieval from Sentinel-5 Precursor/TROPOMI using FP\_ILM, *Atmos. Meas. Tech. Discuss.*, 12, 5503–5517, <https://doi.org/10.5194/amt-12-5503-2019> submitted, 2019.
- Herman, J. R., and Celarier E. A.: Earth surface reflectivity climatology at 340–380nm from TOMS data, *J. Geophys. Res.*, 102(D23), 28,003–28,011, doi:10.1029/97JD02074, 1997.
- 25 Inness, A., Flemming, J., Heue, K.-P., Lerot, C., Loyola, D., Ribas, R., Valks, P., van Roozendaal, M., Xu, J., and Zimmer, W.: Monitoring and assimilation tests with TROPOMI data in the CAMS system: near-real-time total column ozone, *Atmos. Chem. Phys.*, 19, 3939–3962, <https://doi.org/10.5194/acp-19-3939-2019>, 2019.
- Kleipool, Q., Ludewig, A., Babić, L., Bartstra, R., Braak, R., Dierssen, W., Dewitte, P.-J., Kenter, P., Landzaat, R., Leloux, J., Loots, E., Meijering, P., van der Plas, E., Rozemeijer, N., Schepers, D., Schiavini, D., Smeets, J., Vacanti, G., Vonk, F.,

- and Veefkind, P.: Pre-launch calibration results of the TROPOMI payload on-board the Sentinel-5 Precursor satellite, *Atmos. Meas. Tech.*, 11, 6439-6479, <https://doi.org/10.5194/amt-11-6439-2018>, 2018.
- Kleipool, Q. L., Dobber M. R., de Haan J. F., and Levelt P. F.: Earth surface reflectance climatology from 3 years of OMI data, *J. Geophys. Res.*, 113, D18308, doi:10.1029/2008JD010290, 2008.
- 5 Koelemeijer, R. B. A., de Haan J. F., and Stammes P.: A database of spectral surface reflectivity in the range 335–772nm derived from 5.5 years of GOME observations, *J. Geophys. Res.*, 108(D2), 4070, doi:10.1029/2002JD002429, 2003.
- Labow, G. J., Ziemke, J. R., McPeters, R. D., Haffner, D. P., and Bhartia, P. K.: A total ozone-dependent ozone profile climatology based on ozonesondes and Aura MLS data, *J. Geophys. Res. Atmos.*, 120/6, 2537–2545, 2015.
- Lee, C., R. V. Martin, A. van Donkelaar, G. O'Byrne, A. Richter, G. Huey, and J. S. Holloway, Retrieval of vertical columns  
10 of sulfur dioxide from SCIAMACHY and OMI: Air mass factor algorithm development and validation, *J. Geophys. Res.*, 114, D22303, doi:[10.1029/2009JD012123](https://doi.org/10.1029/2009JD012123), 2009.
- Lin, J.-T., Martin, R. V., Boersma, K. F., Sneep, M., Stammes, P., Spurr, R., Wang, P., Van Roozendaal, M., Clémer, K., and Irie, H.: Retrieving tropospheric nitrogen dioxide from the Ozone Monitoring Instrument: effects of aerosols, surface reflectance anisotropy, and vertical profile of nitrogen dioxide, *Atmos. Chem. Phys.*, 14, 1441–1461,  
15 <https://doi.org/10.5194/acp-14-1441-2014>, 2014.
- Lerot C., Van Roozendaal M., Spurr R., Loyola D., Coldewey-Egbers M., Kochenova S., van Gent J., Koukouli M., Balis D., Lambert J.-C., Granville J., Zehner C., Homogenized total ozone data records from the European sensors GOME/ERS-2, SCIAMACHY/Envisat, and GOME-2/MetOp-A, *Journal of Geophysical Research*, 119, 1639–1662, doi:[10.1002/2013JD020831](https://doi.org/10.1002/2013JD020831), 2014.
- 20 Lerot C., Van Roozendaal M., Lambert J.-C., Granville J., Van Gent J., Loyola D., Spurr R. J. D., The GODFIT algorithm: a direct fitting approach to improve the accuracy of total ozone measurements from GOME, *International Journal of Remote Sensing*, 31:2, 543–550, doi:[10.1080/01431160902893576](https://doi.org/10.1080/01431160902893576), 2010.
- Lorente, A., Boersma, K. F., Stammes, P., Tilstra, L. G., Richter, A., Yu, H., Kharbouche, S., and Muller, J.-P.: The importance of surface reflectance anisotropy for cloud and NO<sub>2</sub> retrievals from GOME-2 and OMI, *Atmos. Meas. Tech.*, 11,  
25 4509-4529, <https://doi.org/10.5194/amt-11-4509-2018>, 2018.
- Loyola, D. G., Heue, K.-P., Xu, J., Zimmer, W., and Romahn, F. et al.: The near-real-time total ozone retrieval algorithm from TROPOMI onboard Sentinel-5 Precursor, *Atmos. Meas. Tech. Discuss.*, in preparation, 2019.
- Loyola, D. G., Gimeno García, S., Lutz, R., Argyrouli, A., Romahn, F., Spurr, R. J. D., Pedernana, M., Doicu, A., Molina García, V., and Schüssler, O.: The operational cloud retrieval algorithms from TROPOMI on board Sentinel-5 Precursor,  
30 *Atmos. Meas. Tech.*, 11, 409-427, <https://doi.org/10.5194/amt-11-409-2018>, 2018.

- Loyola, D., Pedernana, M., and Gimeno García, S., Smart sampling and incremental function learning for very large high dimensional data, *Neural Networks*, 78, 75–87, <https://doi.org/10.1016/j.neunet.2015.09.001>, 2016.
- Loyola, D., Thomas, W., Spurr, R., and Mayer, B.: Global patterns in daytime cloud properties derived from GOME backscatter UV-VIS measurements", *International Journal of Remote Sensing*, 31:16, 4295-4318, 2010.
- 5 Loyola, D., M. Koukouli, P. Valks, D. Balis, N. Hao, M. Van Roozendael, R. Spurr, W. Zimmer, S. Kiemle, C. Lerot, and J. C. Lambert, The GOME-2 Total Column Ozone Product: Retrieval Algorithm and Ground-Based Validation, *J. Geophys. Res.*, 116, D07302, doi:[10.1029/2010JD014675](https://doi.org/10.1029/2010JD014675), 2011.
- Loyola D.: Applications of Neural Network Methods to the Processing of Earth Observation Satellite Data, *Neural Networks*, 19/2, 168-177, <https://doi.org/10.1016/j.neunet.2006.01.010>, 2006.
- 10 Lutz, R., Loyola, D., Gimeno García, S., and Romahn, F.: OCRA radiometric cloud fractions for GOME-2 on MetOp-A/B, *Atmos. Meas. Tech.*, 9, 2357-2379, <https://doi.org/10.5194/amt-9-2357-2016>, 2016.
- [Mateer, C. L., D. F. Heath, A. J. Krueger: Estimation of Total Ozone from Satellite Measurements of Backscattered Ultraviolet Earth Radiance, J. Atmos. Sci., 28, 1307-1311, https://doi.org/10.1175/1520-0469\(1971\)028<1307:EOTOFS>2.0.CO;2, 1971.](https://doi.org/10.1175/1520-0469(1971)028<1307:EOTOFS>2.0.CO;2)
- 15 [McPeters, R. D., Frith, S., and Labow, G. J.: OMI total column ozone: extending the long-term data record, Atmos. Meas. Tech., 8, 4845–4850, https://doi.org/10.5194/amt-8-4845-2015, 2015.](https://doi.org/10.5194/amt-8-4845-2015)
- [Noguchi, K., Richter, A., Rozanov, V., Rozanov, A., Burrows, J. P., Irie, H., and Kita, K.: Effect of surface BRDF of various land cover types on geostationary observations of tropospheric NO<sub>2</sub>, Atmos. Meas. Tech., 7, 3497–3508, https://doi.org/10.5194/amt-7-3497-2014, 2014.](https://doi.org/10.5194/amt-7-3497-2014)
- 20 [Rozemeijer N.C., Kleipool Q.: S5P Level 1b Product Readme File, S5P-MPC-KNMI-PRF-L1B available at: https://sentinel.esa.int/web/sentinel/technical-guides/sentinel-5p/products-algorithms](https://sentinel.esa.int/web/sentinel/technical-guides/sentinel-5p/products-algorithms) and <http://www.tropomi.eu/documents/level-2-products>, 2019.
- Seidel, F. C. and Popp, C.: Critical surface albedo and its implications to aerosol remote sensing, *Atmos. Meas. Tech.*, 5, 1653-1665, <https://doi.org/10.5194/amt-5-1653-2012>, 2012.
- 25 [Siddans, R., S5P-NPP Cloud Processor ATBD, S5P-NPPC-RAL-ATBD-0001 available at: https://sentinel.esa.int/web/sentinel/technical-guides/sentinel-5p/products-algorithms](https://sentinel.esa.int/web/sentinel/technical-guides/sentinel-5p/products-algorithms) and <http://www.tropomi.eu/documents/atbd>, 2016.
- [Tilstra L. G., O. N. E. Tuinder, P. Wang, and P. Stammes, Surface reflectivity climatologies from UV to NIR determined from Earth observations by GOME-2 and SCIAMACHY, J. Geophys. Res. Atmos., 122, 4084-4111, doi:10.1002/2016JD025940, 2017.](https://doi.org/10.1002/2016JD025940)
- 30

O'Byrne, G., R. V. Martin, A. van Donkelaar, J. Joiner, and E. A. Celarier, Surface reflectivity from the Ozone Monitoring Instrument using the Moderate Resolution Imaging Spectroradiometer to eliminate clouds: Effects of snow on ultraviolet and visible trace gas retrievals, *J. Geophys. Res.*, 115, D17305, doi:[10.1029/2009JD013079](https://doi.org/10.1029/2009JD013079), 2010.

5 Pedernana, M., Loyola, D., Apituley, A., Sneep, M., Veefkind, J. P.: Sentinel-5 precursor/TROPOMI – Level 2 Product User Manual – Ozone Total Column, S5P-L2-DLR-PUM-400A available at: <https://sentinel.esa.int/web/sentinel/technical-guides/sentinel-5p/products-algorithms> and <http://www.tropomi.eu/documents/level-2-productsatbd>, 2018.

Pflug B., Aberle B., Loyola D., Valks P., Near-Real-Time Estimation of Spectral Surface Albedo from GOME-2/MetOp Measurements, EUMETSAT Meteorological Satellite Conference, Darmstadt, September, 2008.

10 Qin, W., Fasnacht, Z., Haffner, D., Vasilkov, A., Joiner, J., Krotkov, N., Fisher, B., and Spurr, R.: A geometry-dependent surface Lambertian-equivalent reflectivity product at 466 nm for UV/Vis retrievals: – Part 1: Evaluation over land surfaces using measurements from OMI at 466 nm, *Atmos. Meas. Tech. Discuss.*, 12, 3997–4017, <https://doi.org/10.5194/amt-12-3997-2019><https://doi.org/10.5194/amt-2018-327>, in review, 2019.

15 De Smedt, I., Theys, N., Yu, H., Danckaert, T., Lerot, C., Compennolle, S., Van Roozendael, M., Richter, A., Hilboll, A., Peters, E., Pedernana, M., Loyola, D., Beirle, S., Wagner, T., Eskes, H., van Geffen, J., Boersma, K. F., and Veefkind, P.: Algorithm theoretical baseline for formaldehyde retrievals from S5P TROPOMI and from the QA4ECV project, *Atmos. Meas. Tech.*, 11, 2395-2426, <https://doi.org/10.5194/amt-11-2395-2018>, 2018.

Spurr, R. J. D. VLIDORT: A linearized pseudo-spherical vector discrete ordinate radiative transfer code for forward model and retrieval studies in multilayer multiple scattering media, *J. Quant. Spectrosc. Radiat. Transf.*, 102, 316-42, doi:[10.1016/j.jqsrt.2006.05.005](https://doi.org/10.1016/j.jqsrt.2006.05.005), 2006.

20 [Spurr R., de Haan J., van Oss R., Vasilkov A.: Discrete-ordinate radiative transfer in a stratified medium with first-order rotational Raman scattering, \*Journal of Quantitative Spectroscopy and Radiative Transfer\*, 109 \(3\), 404-425, 2008.](#)

Rault, D. F., and G. Taha, Validation of ozone profiles retrieved from Stratospheric Aerosol and Gas Experiment III limb scatter measurements, *J. Geophys. Res.*, 112, D13309, doi:[10.1029/2006JD007679](https://doi.org/10.1029/2006JD007679), 2007.

25 Theys, N., De Smedt, I., Yu, H., Danckaert, T., van Gent, J., Hörmann, C., Wagner, T., Hedelt, P., Bauer, H., Romahn, F., Pedernana, M., Loyola, D., and Van Roozendael, M.: Sulfur dioxide retrievals from TROPOMI onboard Sentinel-5 Precursor: algorithm theoretical basis, *Atmos. Meas. Tech.*, 10, 119-153, <https://doi.org/10.5194/amt-10-119-2017>, 2017.

Tilstra, L. G., Tuinder O. N. E., Wang P., and Stammes P.: Surface reflectivity climatologies from UV to NIR determined from Earth observations by GOME-2 and SCIAMACHY, *J. Geophys. Res. Atmos.*, 122, 4084–4111, doi:[10.1002/2016JD025940](https://doi.org/10.1002/2016JD025940), 2017.

- Vasilkov, A., Yang, E.-S., Marchenko, S., Qin, W., Lamsal, L., Joiner, J., Krotkov, N., Haffner, D., Bhartia, P. K., and Spurr, R.: A cloud algorithm based on the O<sub>2</sub>-O<sub>2</sub> 477 nm absorption band featuring an advanced spectral fitting method and the use of surface geometry-dependent Lambertian-equivalent reflectivity, *Atmos. Meas. Tech.*, 11, 4093-4107, <https://doi.org/10.5194/amt-11-4093-2018>, 2018.
- 5 Vasilkov, A., Qin, W., Krotkov, N., Lamsal, L., Spurr, R., Haffner, D., Joiner, J., Yang, E.-S., and Marchenko, S.: Accounting for the effects of surface BRDF on satellite cloud and trace-gas retrievals: a new approach based on geometry-dependent Lambertian equivalent reflectivity applied to OMI algorithms, *Atmos. Meas. Tech.*, 10, 333-349, <https://doi.org/10.5194/amt-10-333-2017>, 2017.
- Verhoelst, T., Granville, J., Lambert, J.-C., Heue, K.-P., S5P MPC VDAF Validation Web Article: Total Column of Ozone, 10 S5P-MPC-VDAF-WVA-L2\_O3\_20180720 available at: <http://mpc-vdaf.tropomi.eu/index.php/ozone>, 2018.
- Xu, J., Schüssler, O., Loyola R, D., Romahn, F. and Doicu, A.: A novel ozone profile shape retrieval using Full-Physics Inverse Learning Machine (FP\_ILM). *IEEE J. Sel. Topics Appl. Earth Observ. Remote Sens.* 10(12), pp. 5442–5457, doi: 10.1109/JSTARS.2017.2740168, 2017.
- Zhou, Y., Brunner, D., Spurr, R. J. D., Boersma, K. F., Sneep, M., Popp, C., and Buchmann, B.: Accounting for surface 15 reflectance anisotropy in satellite retrievals of tropospheric NO<sub>2</sub>, *Atmos. Meas. Tech.*, 3, 1185-1203, <https://doi.org/10.5194/amt-3-1185-2010>, 2010.

Table 4: Ranges ~~of for~~ the input parameters ~~appropriate used~~ for radiance simulations in the total ozone fitting window; ~~the~~ ozone profiles are classified as ~~a~~ function of the total column. Smart sampling is ~~employed used~~ to generate node points optimally covering all input dimensions and more than  $2 \times 10^5$  synthetic UV spectra are generated.

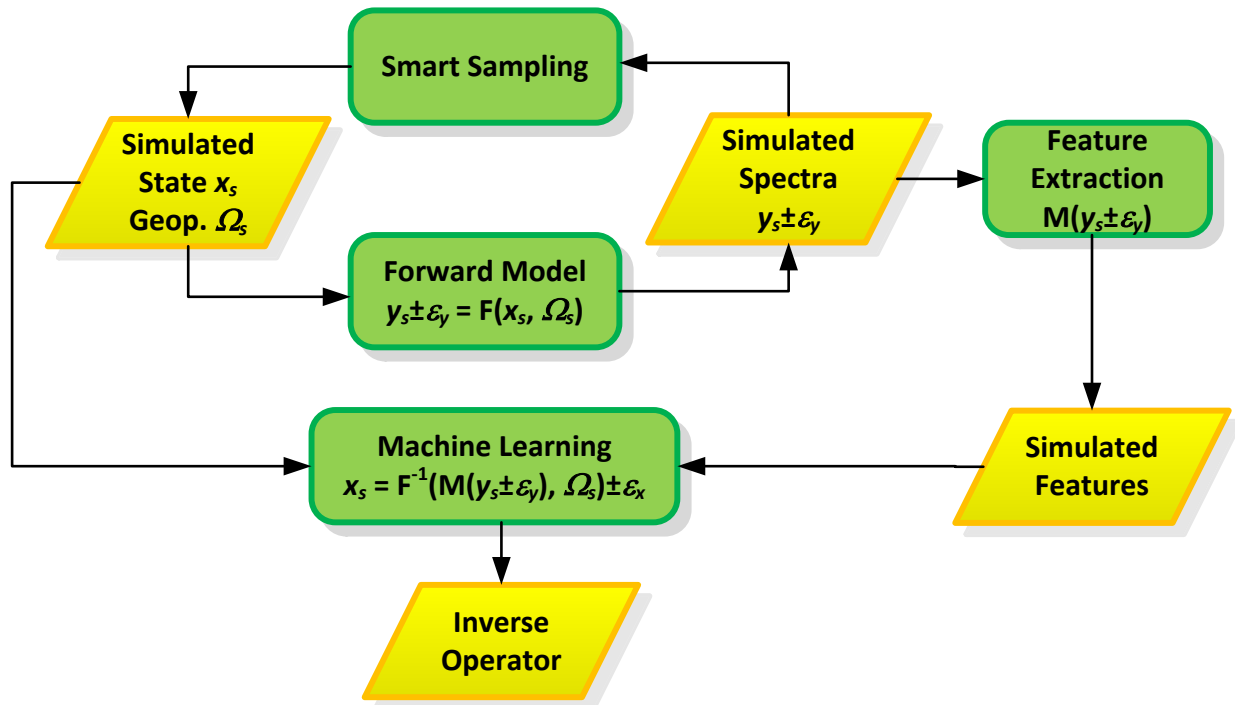
Parameter	Minimum	Maximum
Ozone Profile	125 DU	575 DU
Solar Zenith Angle	0°	90°
Viewing Zenith Angle	0°	70°
Relative Azimuth Angle	0°	180°
Surface Albedo	0	1
Surface Pressure	125 hPa	1013 hPa

Table 5: Summary of the comparison between TROPOMI GE\_LER clear-sky and OMI LER (first three rows) and between ~~as well as for~~ TROPOMI GE\_LER cloudy and ROCINN\_CRB cloud albedo (rows 4-6). There are more than 4.5 million clear-sky and more than 1.4 million cloudy cases out of ~~approximately the around~~ 15 million S5P measurements ~~from in~~ April 10<sup>th</sup>, 2018.

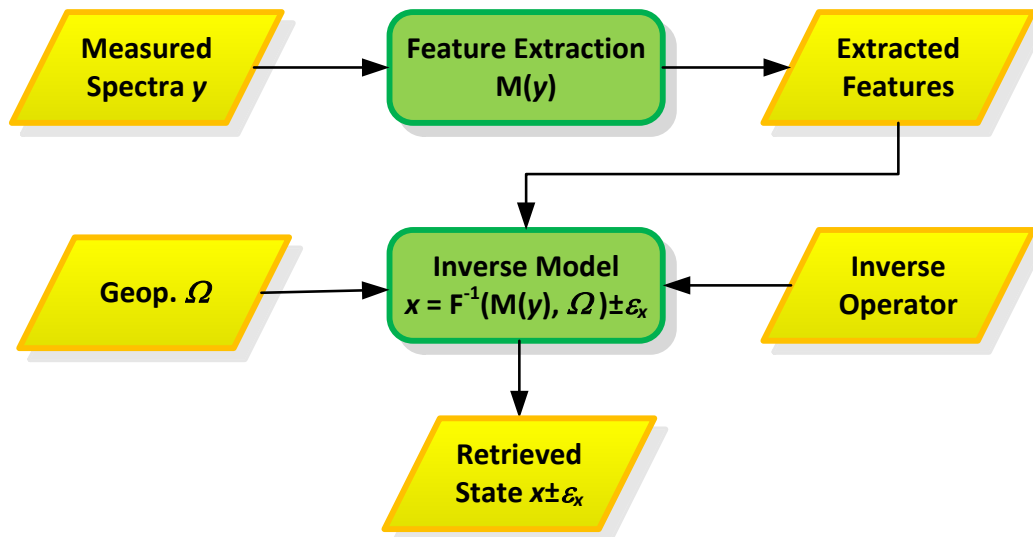
	Number	Mean	Std. Dev.
Clear-sky Land	866 907	0.0014	0.0624
Clear-sky Water	1 837 686	-0.0144	0.0762
Clear-sky Snow/Ice	1 852 222	-0.0048	0.2573
Cloudy Land	254 645	0.0834	0.1865
Cloudy Water	1 084 985	0.0487	0.1464
Cloudy Snow/Ice	127 636	-0.0343	0.5432

Table 6: Latitudinal differences between total ozone from CAMS and S5P using TROPOMI G3\_LER and OMI LER for the complete-month of April 2018. The values represent the total number of measurements for each latitudinal range and the mean differences  $\pm$  standard deviations (in percentages). Latitude bands with less than 100000 data points/degree were skipped, due to the polar winter conditions, there are hardly any data south of 81°S. The number of measurements increases towards higher in the north because of the overlapping orbits.

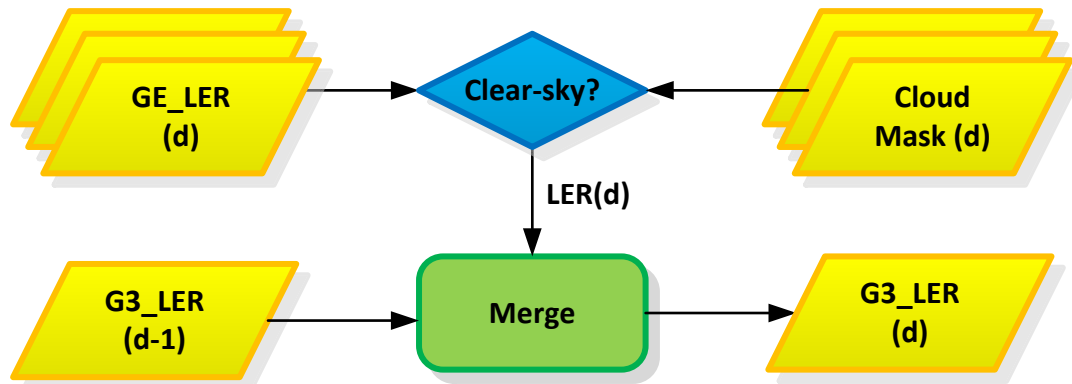
Latitude Range	Number	TROPOMI G3_LER	OMI LER
80°S-70°S	11297206	<u>-1.341 <math>\pm</math> 2.364</u>	-2.041 $\pm$ 2.114
70°S-60°S	29018428	<u>-0.364 <math>\pm</math> 2.472</u>	-2.727 $\pm$ 2.300
60°S-50°S	32351377	<u>0.557 <math>\pm</math> 1.783</u>	0.808 $\pm$ 1.815
50°S-40°S	31580917	<u>-0.345 <math>\pm</math> 1.189</u>	0.048 $\pm$ 1.224
40°S-30°S	31154717	<u>-0.776 <math>\pm</math> 0.906</u>	-0.336 $\pm$ 0.930
30°S-20°S	30948143	<u>-0.726 <math>\pm</math> 0.770</u>	-0.252 $\pm$ 0.807
20°S-10°S	30814933	<u>-0.001 <math>\pm</math> 0.736</u>	0.537 $\pm$ 0.745
10°S-0°S	30744238	<u>-0.163 <math>\pm</math> 0.774</u>	0.517 $\pm$ 0.720
0°N-10°N	30732173	<u>-0.199 <math>\pm</math> 0.833</u>	0.607 $\pm$ 0.738
10°N-20°N	30779225	<u>-0.581 <math>\pm</math> 0.798</u>	0.142 $\pm$ 0.728
20°N-30°N	30894360	<u>-0.788 <math>\pm</math> 0.945</u>	-0.097 $\pm$ 0.901
30°N-40°N	31091907	<u>-0.710 <math>\pm</math> 1.340</u>	0.173 $\pm$ 1.336
40°N-50°N	31469922	<u>-0.456 <math>\pm</math> 1.858</u>	0.584 $\pm$ 1.880
50°N-60°N	32250750	<u>-0.474 <math>\pm</math> 1.721</u>	1.287 $\pm$ 1.920
60°N-70°N	39590441	<u>-0.977 <math>\pm</math> 2.211</u>	1.155 $\pm$ 2.798
70°N-80°N	56545121	<u>-1.182 <math>\pm</math> 2.581</u>	-0.730 $\pm$ 2.701
80°N-90°N	26178029	<u>-1.717 <math>\pm</math> 2.424</u>	-1.595 $\pm$ 2.317



5 | Figure 14: Data flow diagram ~~of for~~ the FP\_ILM training phase. The smart sampling techniques ~~is used to~~ create simulated state vector  $x_s$  and geophysical conditions  $\Omega_s$  that are used as input to ~~a the~~ forward model for the ~~calculation creation~~ of simulated spectra with their expected errors  $y_s + e_y$ . ~~Machine learning techniques are~~ ~~deployed used~~ for computing the inverse operator that is trained using as input the features extracted from the simulated spectra  $M(y_s)$  and the geophysical conditions  $\Omega_s$  as an output the state vector and the errors  $x_s + e_x$ .



10 Figure 15: Data flow diagram ~~of for~~ the FP\_ILM retrieval phase. The inverse operator computed during the FP\_ILM training phase ~~is used to solve~~ the inverse problem and retrieve the state vector  $x$  taking as input the features  $M(y)$  extracted from the measured spectra  $y$  and ~~the~~ geophysical conditions  $\Omega$ .



5 | Figure 16: Data flow diagram of-for the creation of the global gapless geometry-dependent LER (G3\_LER) map for day  $d$ . obtained by merging the clear-sky LER data from the same day with the G3\_LER map from the previous day.

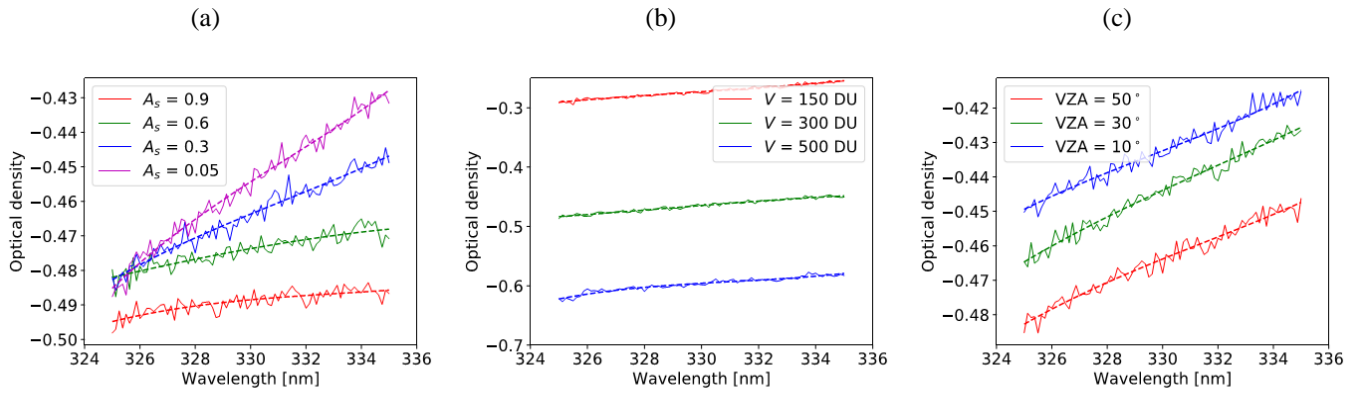


Figure 17: Optical densities difference of the DOAS polynomial as a function of wavelength: with respect to (a) surface albedo, (b) total ozone, and (c) viewing zenith angle. The dotted-lines represent the DOAS fitted polynomial.

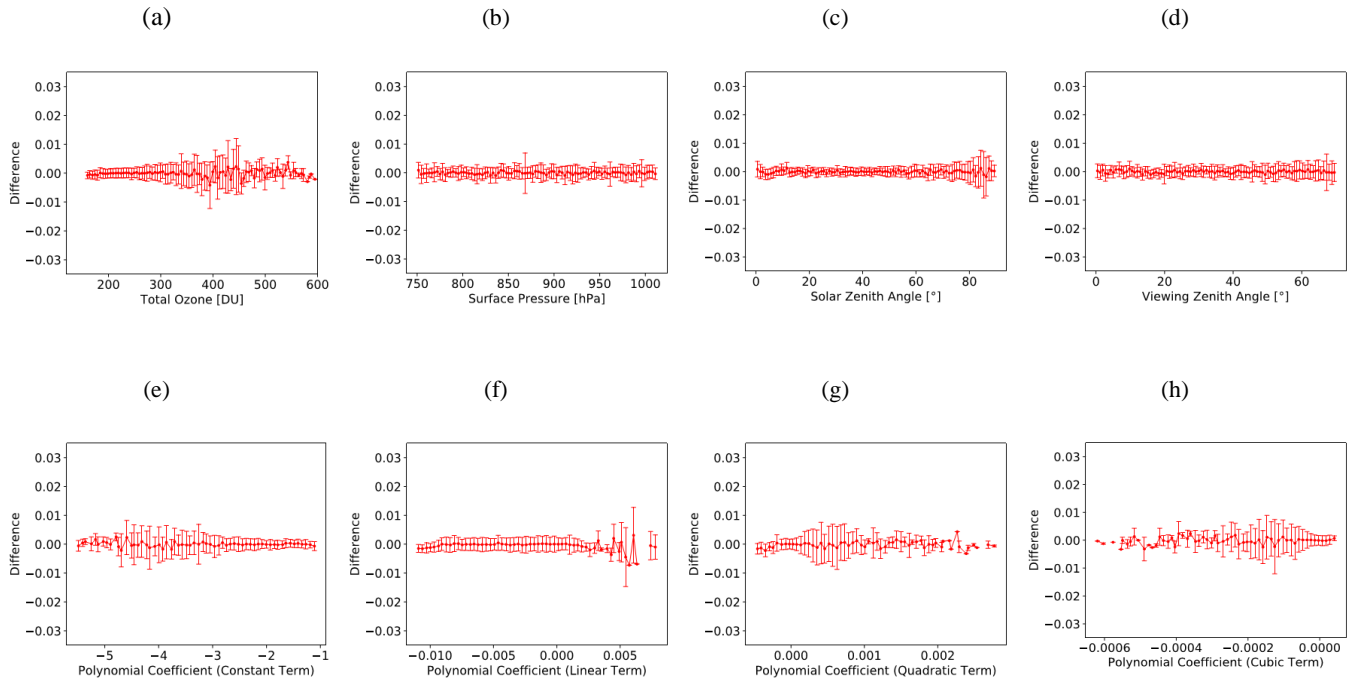


Figure 18: GE\_LER retrieval error as a function of (a) total ozone, (b) surface pressure, (c) solar zenith angle, (d) viewing zenith angle, and (e to h) the four DOAS polynomial fitting coefficients.

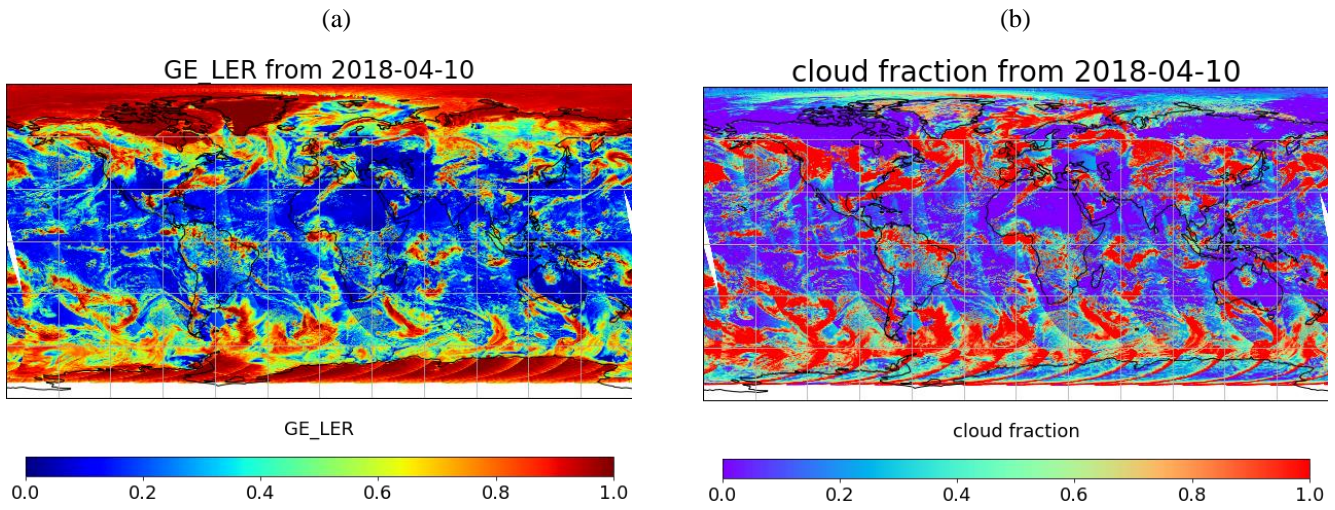
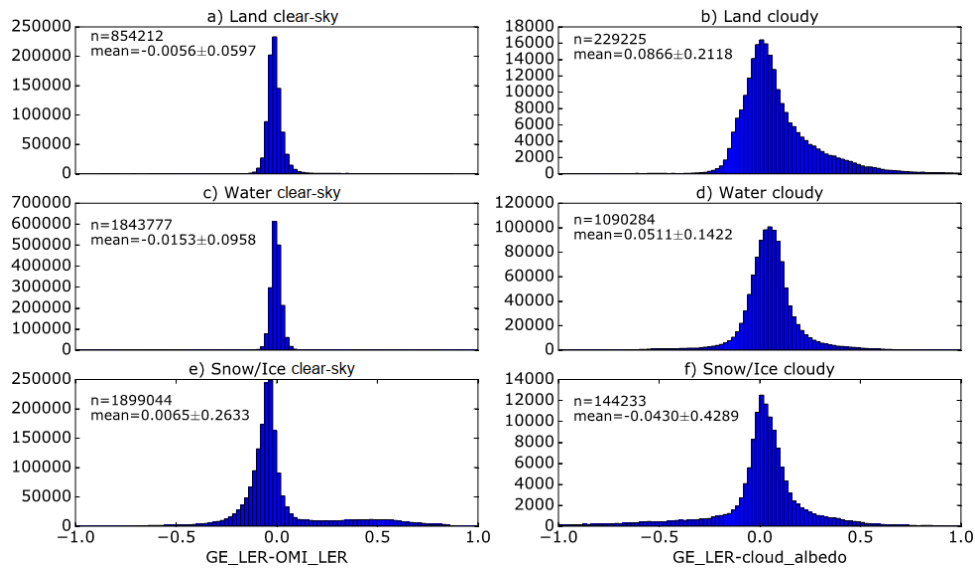


Figure 19: (a) GE\_LER in the total ozone fitting windows [325-335 nm] retrieved from TROPOMI/S5P data ~~from~~on April 10<sup>th</sup>, 2018 and (b) the corresponding cloud fraction for this day.



5 | **Figure 20: Histograms of the differences (left) between clear-sky TROPOMI GE\_LER and OMI LER climatology and (right) between the cloudy TROPOMI GE\_LER and the ROCINN\_CRB cloud albedo from the operational S5P cloud product. The comparisons are performed separately according to per-surface types (land, water, and snow/ice), with and using S5P data from April 10<sup>th</sup> 2018.**

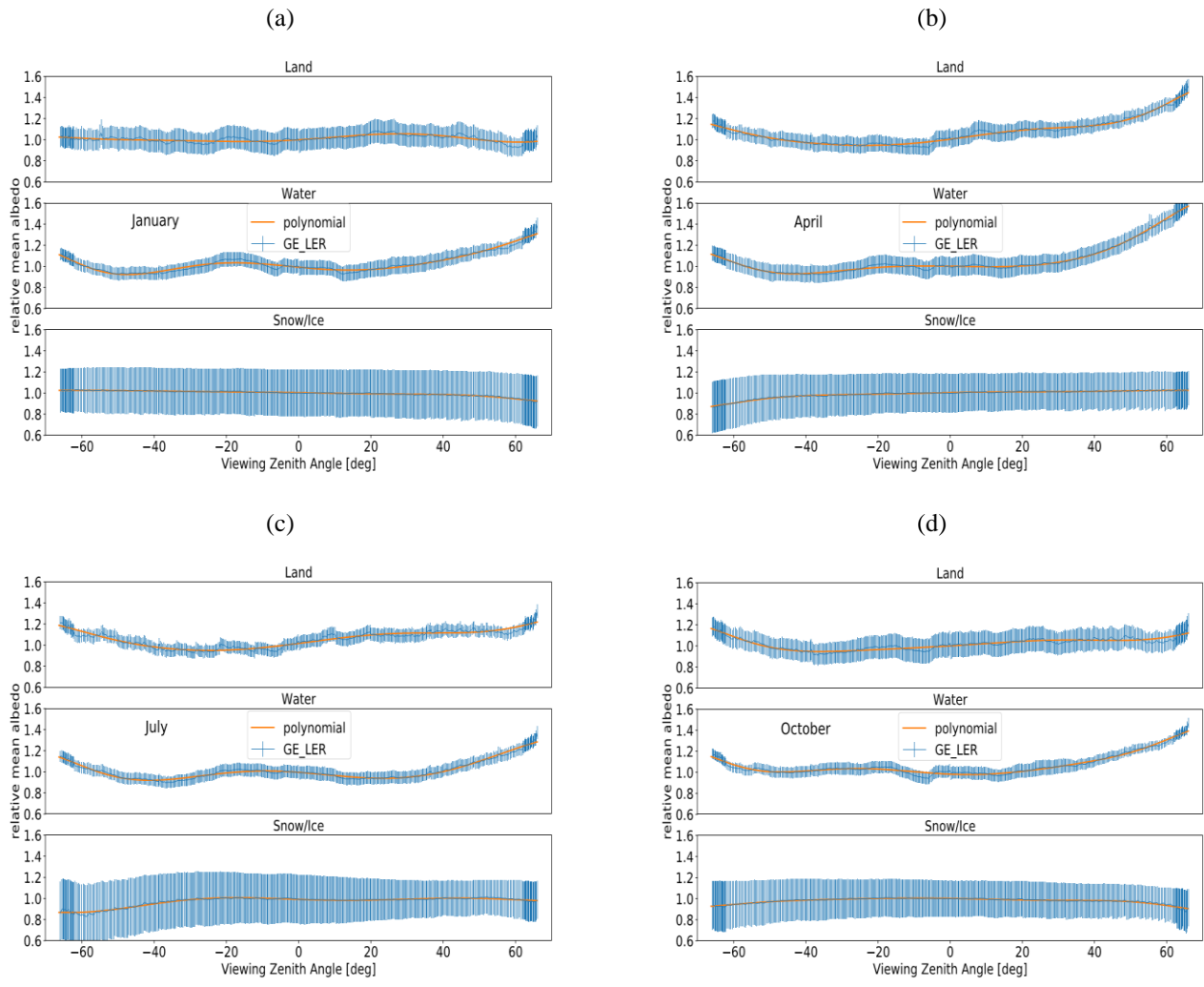


Figure 21: BRDF dependencies  $\rho(\theta)$  as a function of the viewing zenith angle for land, water, and snow/ice conditions, as calculated with normalized TROPOMI/SSP data from (a) January, (b) April, (c) July, and (d) October 2018. The negative viewing zenith angles correspond to the first 225 detector pixels. ~~The discontinuity at nadir is due to numerical issues in the radiative transfer model calculations with very small relative azimuth angles.~~

5

# Albedo maps from 2018-04

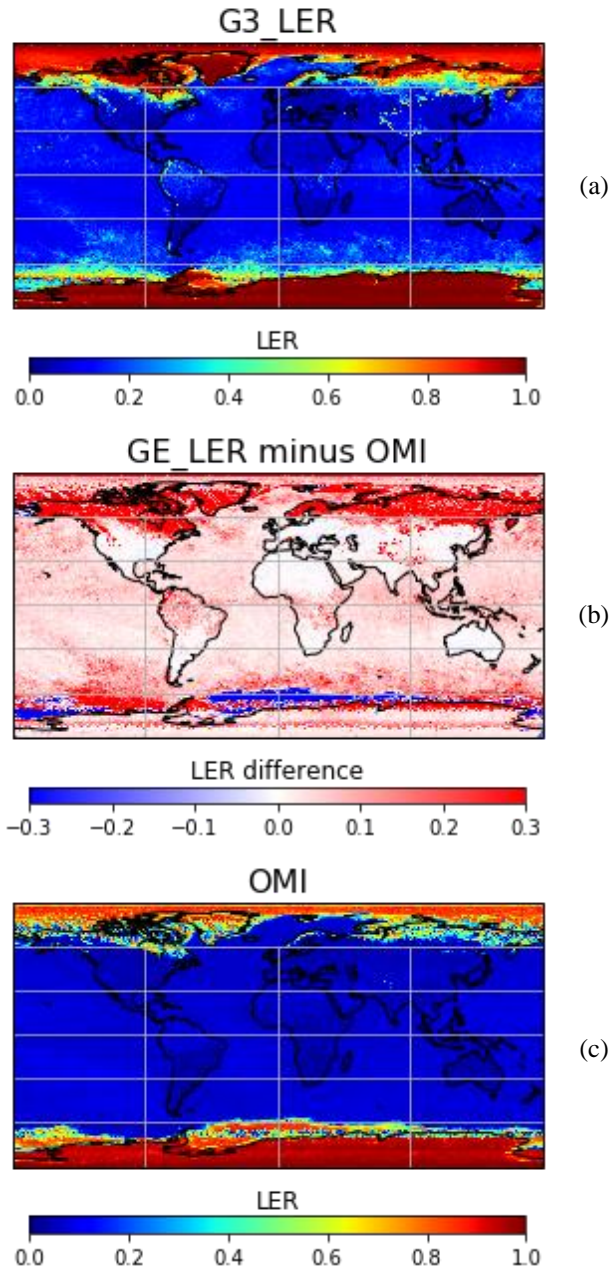
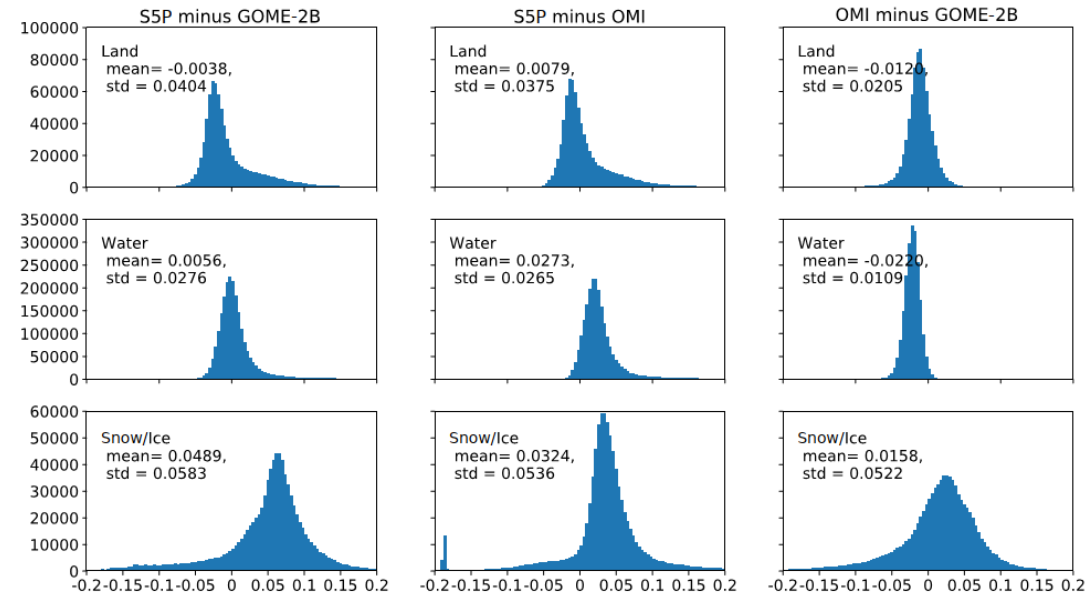


Figure 22: (a) TROPOMI G3\_LER daily map (325-335 nm) for ~~corresponding to~~ April 30<sup>th</sup>, 2018, (c) OMI LER climatology (335 nm) for the month of April, and (b) the difference between these two datasets. There is a very good agreement over land and water surfaces, ~~the~~ with major differences ~~are due to~~ in snow/ice regions ~~in of~~ the OMI LER climatology from 2004-2007 that do not match with ~~the~~ actual surface conditions observed in April 2018.

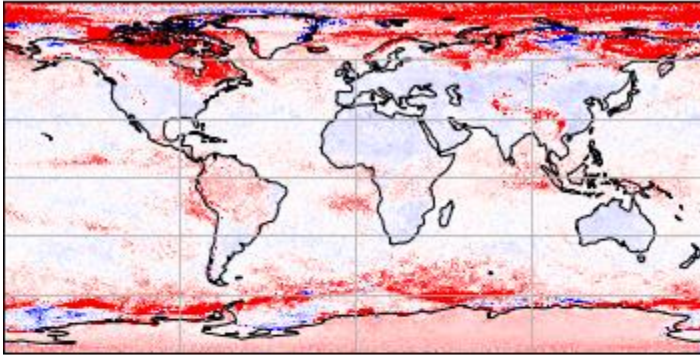


**Figure 23: Histograms of the differences (left) between TROPOMI G3 LER and GOME-2B climatology, (middle) between TROPOMI G3 LER and OMI LER climatology, and (right) between OMI and GOME-2B LER climatologies. The comparisons are performed separately for surface types (land, water, and snow/ice) using data from October 2018.**

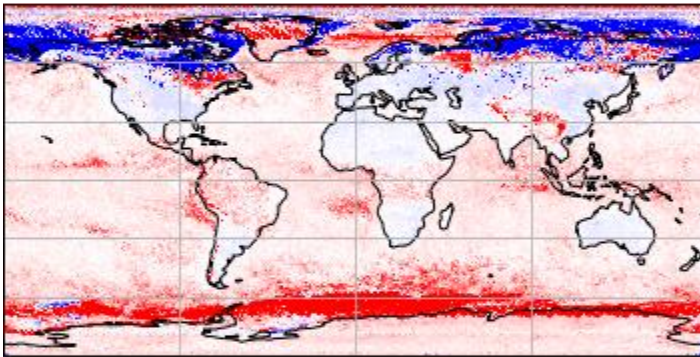
5

## Albedo differences from 2018-10

S5P minus GOME-2B



S5P minus OMI



OMI minus GOME-2B

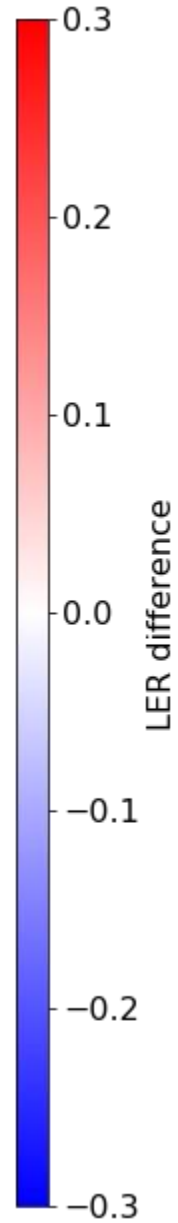
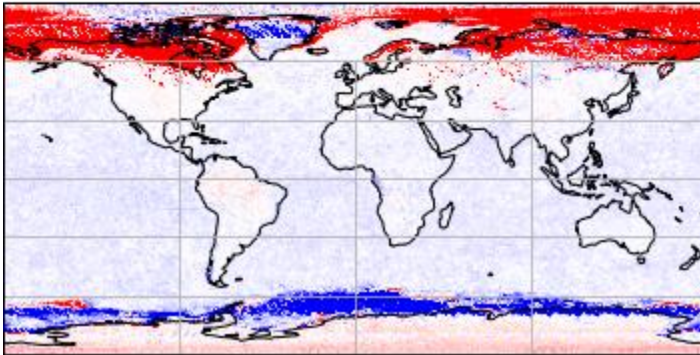


**Figure 24:** Albedo difference maps between TROPOMI, GOME-2 and OMI for October 2018. North of 60°N the discrepancy between the three datasets reaches a maximum due to snow/ice conditions. While S5P overestimates compared to GOME-2, it underestimates compared to OMI.

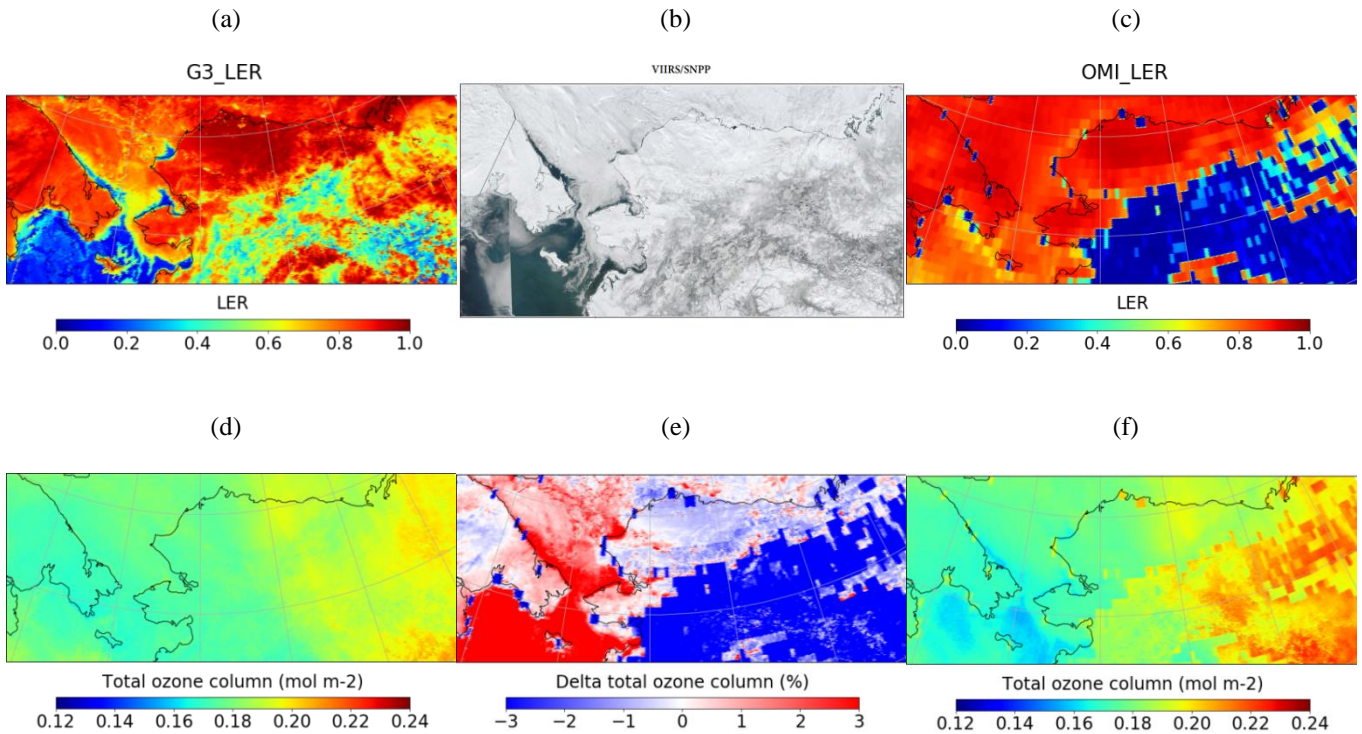
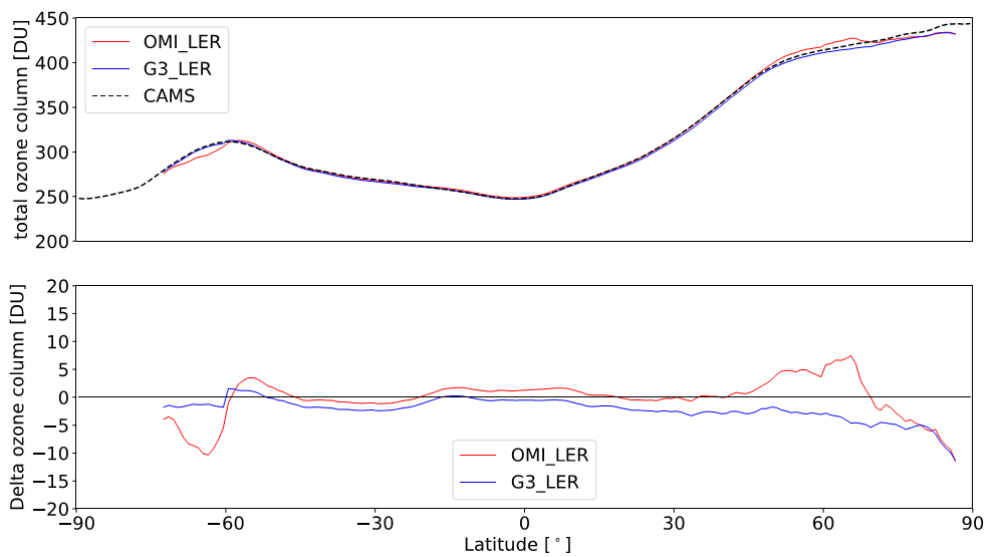


Figure 25: TROPOMI/S5P (top) surface and (bottom) ozone measurements from April 1<sup>st</sup>, 2018 around the Bering Strait. The (a) TROPOMI/S5P G3\_LER daily map agrees very well with the surface types observed in the (b) VIIRS/SNPP image ~~including the water surface along the coastals waters~~ of Russia and Alaska. These ~~coastal waters surfaces along the coast~~ as well as the ~~open waters~~ of the Bering Sea are not properly represented in the (c) OMI LER climatology that shows snow/ice over these regions. Likewise, the OMI LER climatology erroneously shows no snow/ice in Alaska. The total ozone ~~field~~ using the (d) TROPOMI G3\_LER daily map is significantly smoother than the ~~field derived from corresponding one using~~ the (f) OMI LER climatology. The coarse spatial resolution of the OMI LER climatology is clearly ~~manifested visible~~ in the total ozone field and ~~incorrect what is even worst the wrong~~ snow/ice values in the OMI LER climatology induce large errors ~~ei~~n the retrieved total ozone (e) with differences between -10% and +15%.

5

10

5



10

Figure 26: Comparison of total ozone from CAMS and the S5P retrieved ozone using the OMI LER climatology and the daily TROPOMI G3\_LER maps for April 2018. ~~The~~ total ozone values based on daily G3\_LER maps is significantly closer to those from CAMS especially for ~~the~~ high latitude regions.

15